Structural and ligand binding analyses of the periplasmic sensor domain of RsbU in *Chlamydia trachomatis* support a role in TCA cycle regulation

Katelyn R. Soules,[1] Aidan Dmitriev,[1] Scott D. LaBrie,[1] Zoë E. Dimond,[1] Benjamin H. May,[1] David K. Johnson,[2] Yang Zhang,[3] Kevin P. Battaile,[4] Scott Lovell[5] and P. Scott Hefty (iD) [1]*

[1] *Department of Molecular Biosciences, University of Kansas, Lawrence, KS 66045, USA.*
[2] *Computational Chemical Biology Core Facility, Del Shankel Structural Biology Center, University of Kansas, Lawrence, KS 66047, USA.*
[3] *Computational Medicine & Bioinformatics, University of Michigan, Ann Arbor, MI 48109, USA.*
[4] *IMCA-CAT, Hauptman-Woodward Medical Research Institute, Argonne, IL 60439, USA.*
[5] *Protein Structure Laboratory, Del Shankel Structural Biology Center, University of Kansas, Lawrence, KS 66047, USA.*

Summary

Chlamydia trachomatis* is an obligate intracellular bacteria that undergo dynamic morphologic and physiologic conversions upon gaining an access to a eukaryotic cell. These conversions likely require the detection of key environmental conditions and regulation of metabolic activity. *Chlamydia* encodes homologs to proteins in the Rsb phosphoregulatory partner-switching pathway, best described in *Bacillus subtilis*. ORF CT588 has a strong sequence similarity to RsbU cytoplasmic phosphatase domain but also contains a unique periplasmic sensor domain that is expected to control the phosphatase activity. A 1.7 Å crystal structure of the periplasmic domain of the RsbU protein from *C. trachomatis* (PDB 6MAB) displays close structural similarity to DctB from *Vibrio* and *Sinorhizobium*. DctB has been shown, both structurally and functionally, to specifically bind to the tricarboxylic acid (TCA) cycle intermediate succinate. Surface plasmon resonance and differential scanning fluorimetry of TCA intermediates and potential metabolites from a virtual screen of RsbU revealed that alpha-ketoglutarate, malate and oxaloacetate bound to the RsbU periplasmic domain. Substitutions in the putative binding site resulted in reduced binding capabilities. An RsbU null mutant showed severe growth defects which could be restored through genetic complementation. Chemical inhibition of ATP synthesis by oxidative phosphorylation phenocopied the growth defect observed in the RsbU null strain. Altogether, these data support a model with the Rsb system responding differentially to TCA cycle intermediates to regulate metabolism and key differentiation processes.

Introduction

Bacteria possess the ability to sense changes in environmental conditions and adjust biologic activities through diverse regulatory components and mechanisms (Zhulin *et al.*, 2003). Often these reactions are in responses to general environmental stresses as is the case with the regulator of sigma B or Rsb system. This phosphoregulatory partner switching system is found mainly in Firmicutes and is most thoroughly described in *Bacillus subtilis* (Hecker *et al.*, 2007). A central regulatory component in this system is a phosphatase termed RsbU. Under stressful conditions, such as nutrient depletion, RsbU dephosphorylates serine on an intermediate protein partner, RsbV. This allows another protein partner and kinase, RsbW, to 'switch' from association with sigma B to rephosphorylate RsbV. Ultimately, this enables the alternative sigma factor to freely diffuse and form an RNA holoenzyme polymerase, which activates the transcription of over 100 genes that assist with the response to environmental stress (Benson and Haldenwang, 1993; Voelker *et al.*, 1995b; 1995a; Wise and Price, 1995; Kang *et al.*, 1996; Yang *et al.*, 1996; Hughes and Mathee, 1998; Kang *et al.*, 1998). While the Rsb system is typically associated with general stress responses in Firmicutes, it has also been associated with regulating diverse processes in other bacteria phyla including biofilm formation, type

III secretion and swarming motility (Kozak *et al.*, 2005; Morris and Visick, 2013).

Chlamydia undergoes dynamic morphologic and physiologic conversions upon gaining access to a eukaryotic cell. These conversions occur as *Chlamydia* grows and propagates through a phylum-defining biphasic developmental cycle. The initial phase of the chlamydial developmental cycle is the conversion from an infectious, nonreplicative and metabolically inert form known as an elementary body (EB) to a noninfectious, metabolically active and replicative form, known as a reticulate body (RB). This conversion occurs upon gaining access to the cell and establishing the intracellular vacuole termed as inclusion (Elwell *et al.*, 2016). During the EB to RB conversion, many ATP-requiring processes occur, including *de novo* transcription and translational activity, as well as protein secretion. RBs also need to acquire most macromolecules from the host cell, including glucose-6-phosphate, nucleotides, amino acids, lipids and other metabolic precursors for growth and multiple rounds of replication (Mehlitz *et al.*, 2017). The second phase is the asynchronous RB to EB conversion which occurs later in the developmental cycle through unknown signals and poorly understood mechanisms. This conversion also requires coordinated events that include membrane remodeling and infectious capability preparation, while metabolic processes, including transcription and translation, are silenced (Hatch *et al.*, 1984; Hackstadt *et al.*, 1985). *Chlamydia* also organizes the escape from the infected host cell through either cell lysis or extruding vacuoles which enables the infection of new cells and possible a new host.

Chlamydia appears to acquire ATP from the host cell using ATP translocases and can also generate ATP through unique substrate-level and oxidative phosphorylation processes. Interestingly, these processes appear to be functional at different developmental stages. ATP stored in EBs may allow for initial protein secretion and transcription and translation processes to occur until RB conversion. After the initial entry into the host cell, ATP translocases are utilized to obtain ATP from the host cell (Liang *et al.*, 2018). During the RB replication and mid-cycle growth stage, Liang *et al.* (2018) demonstrated that *Chlamydia* can also generate ATP using a sodium-ion gradient to drive the ATP-synthase (Liang *et al.*, 2018). Critical for this process is the TCA cycle (Liang *et al.*, 2018). *Chlamydia* spp. lack three canonical TCA enzymes: citrate synthase (*gltA*), aconitase (*acn*) and isocitrate dehydrogenase (*icd*) (Stephens *et al.*, 1998; Iliffe-Lee and McClarty, 1999). Due to the absence of these enzymes, *Chlamydia* possesses a truncated TCA cycle that starts with alpha-ketoglutarate and ends with oxaloacetate that can then be shuttled to other metabolic pathways (Mehlitz *et al.*, 2017). This truncated TCA cycle does enable the chlamydial RBs

to generate NADH, which drives the sodium-dependent NADH dehydrogenase and, subsequently, ATP generation (Liang *et al.*, 2018). However, because of the incomplete TCA cycle, *Chlamydia* must scavenge dicarboxylate intermediates, such as glutarate and alpha-ketoglutarate, from the host cell (Stephens *et al.*, 1998; Iliffe-Lee and McClarty, 1999; 2000). Consequently, there are substantial interactions between the parasitic chlamydial cells and the infected host cell. The intimate association between the host and chlamydial metabolisms suggests that signaling pathways in *Chlamydia* responding to the host's metabolic milieu play critical roles in development and pathogenesis. Despite the likely importance of these signals, much of the basic biology of these pathways remains poorly understood, including the signal for the EB-to-RB conversion, mechanisms for sensing environmental stimuli and the differential regulation of ATP acquisition.

A partner-switching pathway with similarities to the Rsb regulatory pathway could be a primary mechanism for *Chlamydia* to sense environmental conditions and regulate metabolic activity (Stephens *et al.*, 1998). The chlamydial genome encodes genes for the production of RsbU (CT588), RsbV$_1$ (CT424), RsbV$_2$ (CT765) and RsbW (CT549) proteins (Fig. 1) (Stephens *et al.*, 1998). However, there are distinct differences from the canonical Rsb system in *B. subtilis*. For one, chlamydial RsbU is a transmembrane protein situated in the inner membrane with a periplasmic sensor domain attached to a cytoplasmic phosphatase domain (Fig. 2) (Douglas and Hatch, 2000; Hua *et al.*, 2006; Thompson *et al.*, 2015). In contrast, RsbU in *B. subtilis* is strictly cytoplasmic and do not contain a sensor domain, only possessing a phosphatase domain. It is expected that the chlamydial RsbU sensor domain is critical for controlling the phosphatase activity and downstream regulatory processes. Chlamydial RsbU has been shown to dephosphorylate RsbV$_1$ but not RsbV$_2$ (Thompson *et al.*, 2015). Importantly, multiple studies on the biological and functional outcomes of the terminal component and kinase, RsbW support binding and inhibiting the primary sigma factor, σ[66] (Douglas and Hatch, 2000; Hua *et al.*, 2006; Thompson *et al.*, 2015). The expected result of this activity would be a global shutdown of the most transcription in *Chlamydia*.

To discover the potential binding ligands and response regulatory role of the Rsb system in *Chlamydia,* a crystal structure of the RsbU periplasmic domain was determined. This structure was used to identify structurally similar proteins for putative function predictions as well as direct virtual and experimental ligand-binding analyses. Growth phenotypes of RsbU null mutant strains and in the presence of chemical inhibitors of key ATP generating functions were evaluated. Together, these observations
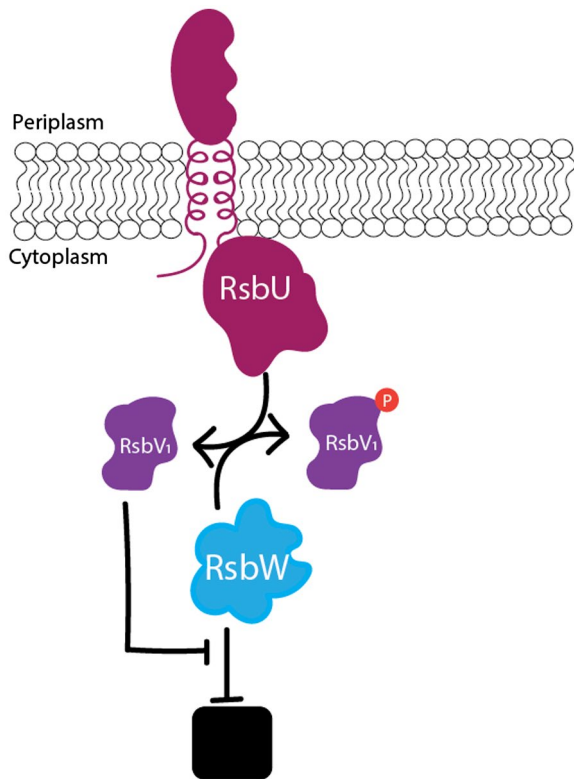
Fig. 1. The current model of the Rsb phospho-switching pathway in *Chlamydia.* RsbW binds and inhibits the activity of a target protein (black box). However, when $RsbV_1$ is dephosphorylated, RsbW will release its target protein to act as a kinase to phosphorylate $RsbV_1$ (Hua *et al.*, 2006; Thompson *et al.*, 2015). RsbU acts as an antagonist of RsbW by dephosphorylating $RsbV_1$ in response to binding a ligand in the periplasm (Thompson *et al.*, 2015). Ultimately, the binding of the ligand to the RsbU protein leads to the release of the target protein.
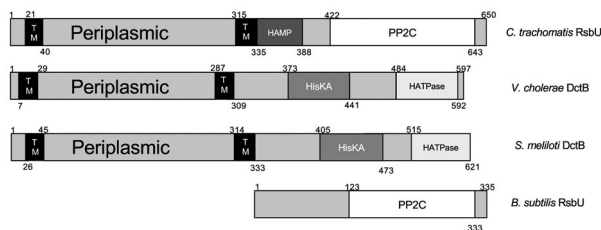

Fig. 2. Domain organization of RsbU from *Chlamydia trachomatis* and homologs from other bacteria. RsbU from *C. trachomatis* bears sequence similarity to RsbU from *B. subtilis* in the cytoplasmic domain, both containing PP2C domains. RsbU in *B. subtilis,* however, does not contain any transmembrane helices, nor a periplasmic portion. Structural comparison of the periplasmic portion of RsbU reveals similarity to the periplasmic domain of DctB proteins in *Vibrio cholerae* and *Sinorhizobium meliloti.* Amino acids are numbered at the beginning and end of domains. TM denotes transmembrane helices.

support that RsbU is binding to TCA cycle intermediates and may play a role in global gene regulation in *Chlamydia.*

Results

CT588 has a unique domain organization with conserved cytoplasmic RsbU phosphatase domain and an uncharacterized domain predicted to localize to the periplasm

CT588 is a 650-residue protein with a carboxyl-terminal domain (269–645) that has high sequence similarity to the RsbU superfamily phosphatases (Fig. 2). This cytoplasmic domain contains HAMP (residues 338–385) and PP2C serine phosphatase (residues 422–625) subdomains with Smart *E*-values of 4.35×10^{-5} and 3.09×10^{-72} respectively (Schultz *et al.*, 1998). The HAMP and PP2C domains together comprise a conserved RsbU family domain (residues 269–645, *E*-value 5.23×10^{-99}) (Schultz *et al.*, 1998) in support of original protein annotation. HAMP domains function as linker regions to modulate the transduction between sensor and effector domains (Hulko *et al.*, 2006). This transduction can occur with cytosolic as well as with membrane-associated proteins (Elliott *et al.*, 2009). PP2C domains are metal-dependent protein phosphatases, which catalyze the dephosphorylation of either a serine or threonine residue (Shi, 2009).

The BLAST search using the N-terminus of CT588 (1-315) revealed sequence similarity to proteins only encoded by *Chlamydia*; however, the predicted function of these orthologs was unknown. In contrast, to other RsbU family members, CT588 has two transmembrane helices that flank residues 40 through 315, which implies that this domain is localized to the periplasm. Based on sequence similarities, it is expected that a periplasmic signal is transduced by the HAMP domain to regulate the PP2C phosphatase activity of CT588. However, while this domain organization of CT588 appears to be unique among bacteria, this protein is widely conserved among the *Chlamydiaceae* family.

I-TASSER was used to model protein structures for the N-terminus RsbU (Yang *et al.*, 2015). Four structural models with relatively poor C-scores (range from −3.19 to −3.84) were generated reflecting the absence of sequence similarity to Protein Data Base (PDB) templates. These models predict two protein domains that are tethered to a single alpha helix, which extends the length of these domains (Fig. S1). Using these models, DALI searches of the PDB were performed to identify potential structural homologs and associated functional information. This search revealed that the top matches (*Z*-score> 15; range 16–21) were all periplasmic-localized chemoreceptors with PAS-like domains attached to kinase or methyl-accepting chemotaxis-like domains by linker regions such as HAMP or HisKA domains from diverse bacteria (Table S1). Many of these I-TASSER model structural homologs also had identified ligands that include L-Arginine, C4-dicarboxylates and asparagine.

A 1.7 Å crystal structure of the RsbU periplasmic domain reveals similarity to periplasmic domains of dicarboxylate binding sensor proteins

A crystal structure of the CT588 (RsbU) periplasmic domain was solved to better understand its function. A construct comprised of residues 45–313 (RsbU$_{45-313}$) was recombinantly expressed and purified via affinity and size exclusion chromatography (Fig. S2) and then used to screen for crystallization conditions which led to a 1.7 Å resolution crystal structure.

RsbU$_{45-313}$ adopts a mixed α/β fold with two similar PAS subdomains, each containing antiparallel β-strands flanked by pairs of α-helices (Fig. 3). The proximal domain contains five long and two short (two residues) β-strands and the distal domain is composed of five long and one short strand. The secondary structure elements for RsbU were calculated using DSSP (Kabsch and Sander, 1983). Interestingly, the proximal and distal subdomains exhibit

a high degree of structural similarity, reflected by a root mean square deviation (RMSD) value of 1.37 Å for 47 aligned C^α atoms (Z = 7.73) (Bryant and Altschul, 1995; Nguyen *et al.*, 2011). Additionally, the total accessible surface area of the subdomains, calculated using Areaimol via CCP4 (Winn *et al.*, 2011) are similar to 5,021.6 Å for the distal (K114-D192) and 5,880.8 Å for the proximal subdomain (K210-E302). Another interesting feature in the RsbU structure is that helix α1 is kinked near I54/T55 (Fig. 3A, right panel). The angle between the two portions of this helix defined by Q45-S53 (α1) and S56-T72 (α1′) was found to be 36.7° as calculated using least-squares fitting of Cα atoms with PyMOL.

A DALI search comparing the RsbU$_{45-313}$ crystal structure to all PDB entries identified 14 nonredundant matches based on the global structural similarity (Z-score> 3.0; Table S2). The top two hits (Z-scores> 15.5) were of the sensor domain from the histidine kinase DctB in *Vibrio*

Fig. 3. Ribbon model of RsbU periplasmic domain (residues 43–313) crystal structure (PDB 6MAB).
A. Tertiary structure showing helices (magenta) and b-sheets (green). The middle and right panels are views rotated 90° and 180° about the vertical direction. The two regions of the kinked helix are denoted as α1 and α1′.
B. Secondary structure annotation is relative to the RsbU sequence.

cholerae and *Sinorhizobium meliloti* (3BY9 and 3E4O respectively), which binds to C_4 di-carboxylates (e.g. succinate). Looking broadly at the domain organization of RsbU from *Chlamydia trachomatis* compared to DctB in *V. cholerae* and *S. meliloti,* these proteins do appear similar in respect to the length of the periplasmic domain and the presence of two flanking transmembrane domains (Fig. 2). DctB is the membrane-bound sensor histidine kinase of a two-component system in Rhizobia, *Vibrio*, *Escherichia* and other bacteria that sense extracellular C_4-dicarboxylates and reactively regulate their TCA cycle, one of the central metabolic processes (Janausch *et al.*, 2002). C_4-dicarboxylates are four-carbon small molecules, such as the TCA cycle intermediates malate and oxaloacetate. Once DctB senses its ligand, it phosphorylates and thereby activates the system's response regulator DctD. Activated DctD then activates the expression of the σ^{54}-dependent promoter of a C_4-dicarboxylate:cation symporter, DctA (Zhou *et al.*, 2008; Nan *et al.*, 2010; Liu *et al.*, 2014). Protein homologs of DctB, each of which is membrane-bound kinases with periplasmic sensor domains, regulate a variety of responses beyond the TCA cycle as well (Cheung and Hendrickson, 2008; Chang *et al.*, 2010; Liu *et al.*, 2015).

Nine of the other matches from the DALI search were structures with bound ligands. These ligands range from amino acids and other carboxylates to nucleic acids. The remaining three protein matches have no ligands solved in their binding sites. These 14 structural matches all are predicted to be membrane-bound proteins with PAS-like domains attached to kinase or methyl-accepting chemotaxis-like domains by linker regions such as HAMP or HisKA domains (Schultz *et al.*, 1998). They regulate a variety of downstream processes such as chemotaxis, sporulation and differential metabolite utilization (Cheung and Hendrickson, 2008; Zhang and Hendrickson, 2010; Wu *et al.*, 2013; Liu *et al.*, 2015; Nishiyama *et al.*, 2016).

Residues in the DctB binding pocket are not conserved in the putative binding pocket of RsbU$_{45-313}$

As noted above, RsbU shares the highest degree of structural similarity with DctB. The superposition of DctB from *V. cholera* (3BY9) and *S. meliloti* (3E4O) with RsbU using Gesamt (Krissinel, 2012) yielded RMSD deviations of 2.58 Å and 3.38 Å between Cα atoms for 205 and 196 residues aligned respectively (Fig. 4A and B). The RMSD deviation between Cα atoms for RsbU and apo DctB (3E4Q) is 3.45 Å (196 residues). Given the structural similarity with DctB, we set out to determine if a similar ligand-binding site was present in RsbU. DctB crystal structures from *V. cholerae* and *S. meliloti* have both been obtained with succinate bound in the ligand-binding
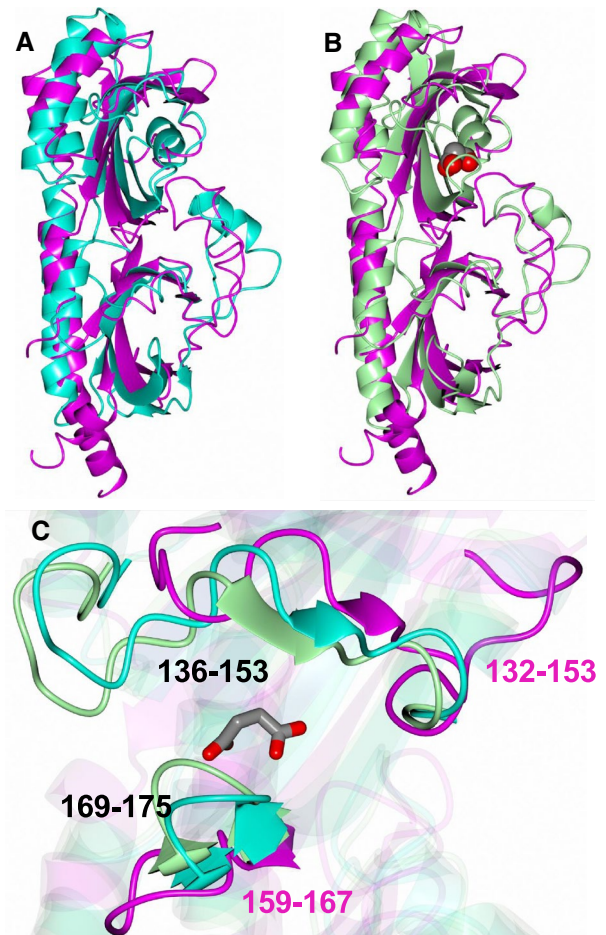

Fig. 4. Superposition of RsbU (6MAB, magenta) with (A) Apo (3E4Q, cyan) and (B) succinate-bound (3E4O, green) DctB structure. The succinate molecule is rendered as spheres to highlight the ligand-binding region. C. Zoomed-in view of the ligand binding pocket with succinate rendered as cylinders. There are evident differences between RsbU and DctB, which is more enclosed. However, structural comparison between the apo and succinate-bound forms of DctB from *Sinorhizobium meliloti* reveals that the linker between strands 3 and 4 (residues 169–175) shift in a distance of 2.2 Å toward the binding pocket when succinate is bound, thereby facilitating pocket enclosure (Zhou *et al*).

pocket (Cheung and Hendrickson, 2008; Zhou *et al.*, 2008). Additionally, a structure of *S. meliloti* DctB has also been obtained as a complex with malonate. Although the structural similarity between RsbU$_{45-313}$ and DctB from *V. cholerae* is greater, the availability of both apo and ligand-bound structures for DctB from *S. meliloti* allowed for a more in-depth comparison with RsbU$_{45-313}$ using these structures. Zhou *et al.* (2008) describe DctB as having an opened apo/C_3-dicarboxylate (malonate) bound structure form and a closed form when bound to a C_4-dicarboxylate. The superposition of RsbU$_{45-313}$ and apo and succinate-bound DctB is depicted in Fig. 4C which highlights the ligand-binding region. Specifically, when DctB binds to a C_4-dicarboxylate, residues 136–153 and 169-175 close

around the ligand. For DctB, the binding of succinate leads to a 2.2 Å movement in residues 169–175 toward the ligand (Zhou *et al.*, 2008). However, for RsbU these loop regions, which correspond to 132-153 and 159-167, are in a more open position, suggesting that a conformational change may occur upon ligand binding.

Despite the structural similarity, there is less than 20% sequence identity between RsbU and DctB sensor domains, particularly around the binding site as a BLAST search yielded no significant conservation of this region. Additionally, the ligand-binding pocket of DctB contains a large patch of positively charged residues whereas RsbU has both positive and negatively charged regions (Fig. 5). Relative to the superimposed structures, S161 and S163 of RsbU are similarly located relative to T171 and S173 of DctB. Additionally, Y142 of RsbU is positioned in a similar location relative to Y149 of DctB. The position of several charged residues within the binding site differs between DctB and RsbU, as highlighted in Fig. 5. In RsbU there are no positively charged residues in the corresponding location of R152 which interacts with succinate (Fig. 5C). Instead, there is a negatively charged residue, E145, located in a similar region. Additionally, K197 of DctB, which is located in the middle β-strand of the binding site β-sheet, forms a salt bridge with the dicarboxylate ligand.

While there is no positively charged residue in the corresponding location on the same β-strand, K114 of RsbU is located in a neighboring β-strand (Fig. 5D). Overall, RsbU contains eight charged residues at or around the putative ligand-binding site. These include negatively charged E145, E115, E250 and positively charged residues K114, R134, K140 and R248 lining the perimeter of the pocket.

I-TASSER ab initio *model of CT588 closely matches the crystal structure*

A pairwise structure comparison of the I-TASSER model and the RsbU$_{1-315}$ structure reveals a robust *Z*-score of 14.4 and RMSD of 4.0 Å (Fig. S1). These data support that, despite extremely low sequence similarity between RsbU$_{1-315}$ and other proteins (maximum sequence similarity below 2% of the templates), I-TASSER was effective in accurately modeling this protein. This *ab initio* protein modeling is particularly challenging, especially for proteins over 200 amino acids (Zhang *et al.*, 2016). Additionally, the comparison between DALI searches of I-TASSER and crystal structure highlights that more than half of the top 15 proteins with structural similarity are shared, including DctB (Table S1).
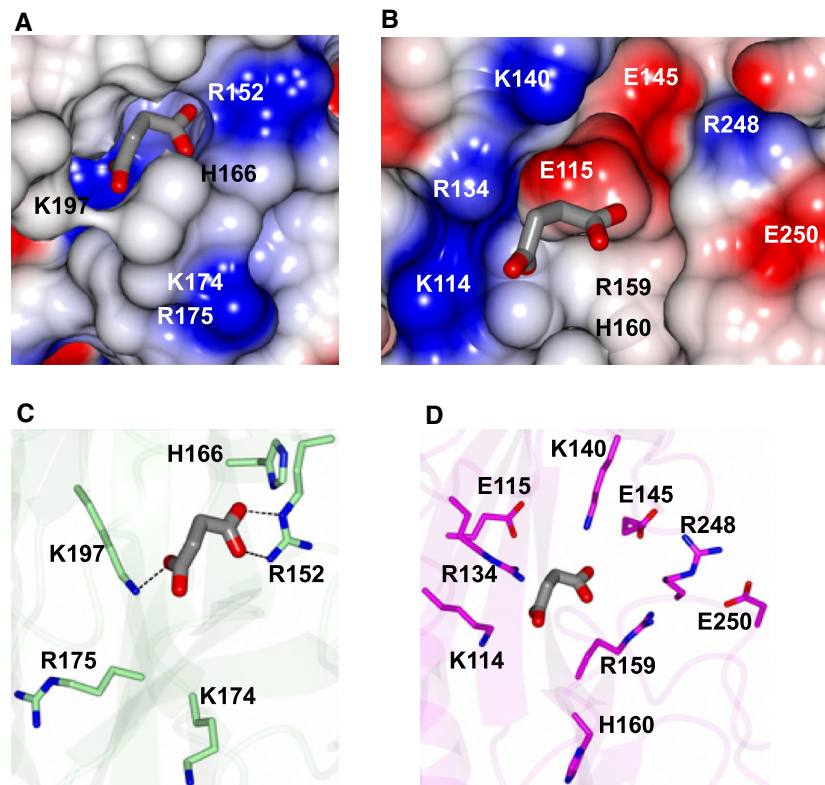

Fig. 5. Residues in the ligand-binding pocket of DctB (3E4O) and putative site of RsbU. The succinate molecule is rendered as gray cylinders.
A. Electrostatic surface for DctB and (B) RsbU. C. Charged residues for DctB showing hydrogen bond interactions with succinate (dashed lines).
D. Charged residues in the putative ligand-binding pocket of RsbU.

Virtual screen of human metabolite and chlamydial metabolite libraries yielded a small list of potential ligands for further testing

While the structure of RsbU is most similar to DctB, it shares the same fold as several other proteins that bind ligands other than dicarboxylates, such as amino acids, nitrogenous bases and pyruvate (Table S3). Preliminary docking studies indicated that the C_4-dicarboxylate succinate could interact with the positively charged side chains of K140 and R134; however, these residues are located in the outer edge of the binding pocket, distal to where a tight-binding ligand would be expected to bind. To rationally select additional compounds for testing, a virtual screen was performed against compounds that are more likely to interact with by RsbU; namely human metabolites and metabolites associated with *C. trachomatis*.

Over 100,000 compounds were computationally screened and a final library of 26 potential ligands was selected for further testing. This library was composed of the top-scoring compounds from the human and chlamydial metabolite libraries supplemented with TCA cycle intermediates or derivatives present in *Chlamydia* (Table S3). The addition of the TCA cycle intermediates or derivatives was included to fully investigate the possibility of the chlamydial RsbU protein binding to a molecule of similar structure and function as the DctB ligand.

Binding studies support TCA cycle intermediates as RsbU ligands

Surface plasmon resonance (SPR) was selected as a method of screening the library of potential ligands for binding to the RsbU$_{45\text{-}313}$ periplasmic domain due to its sensitivity and ability to determine the estimates of binding kinetics (Jason-Moller *et al.*, 2006). In initial screening with the 26 potential ligands at 100 µM and 1 mM concentration, binding was only observed for alpha-ketoglutarate, malate and oxaloacetate (Fig. S3). Subsequently, dose-dependent binding studies of these three potential ligands were performed. K_D values were estimated to be 419 ± 76 µM, 459 ± 91 µM and 396 ± 69 µM for alpha-ketoglutarate, malate and oxaloacetate respectively (Table 1).

Docking with the alpha-ketoglutarate, malate and oxaloacetate to RsbU identified specific residues at the putative binding site that could be coordinating ligand binding (Fig. 6). Residues R134, Q137 and K140 were predicted to interact with alpha-ketoglutarate, malate and oxaloacetate. R248 is also in proximity to the ligands. Based on these predicted residue interactions, individual alanine substitutions in the RsbU$_{45–313}$ protein were created for R134, Q137 and K140, as well as a double substitution with R134 and K140. SPR was performed with the alanine-substituted proteins compared to the wild-type protein. Table 1 shows the average estimated K_D

Table 1. Binding kinetic estimations (µM) for RsbU proteins.

Protein	Alpha-ketoglutarate		Malate		Oxaloacetate	
	K_D	SD	K_D	SD	K_D	SD
WT RsbU$_{45\text{-}313}$	419	76	459	91	396	69
R134A	526	84	601*	62	379	57
Q137A	548	112	666	233	459	96
K140A	597*	120	836*	54	569*	144
K140A/R134A	558*	68	741*	49	580*	97

Abbreviation: SD = Standard deviation.
*P-value < 0.05 when compared to wild-type protein binding by a two-tailed student's *t*-test.

values for the three TCA cycle intermediates with each of the protein variants. Both the signal-substitution variant, K140A, and the double-substitution variant, K140A/R134A, showed statistically significant, albeit limited, decreases in the binding affinity for the three TCA cycle intermediates. The R134A variant displayed a statistically significant decrease in the binding affinity for malate, as well as lower binding capabilities to alpha-ketoglutarate (P-value = 0.082). Similarly, the Q137A single-substitution also had a decrease in the binding affinity for alpha-ketoglutarate and malate (P-value < 0.1).

Orthogonal analyses using differential scanning fluorimetry (DSF) were also performed with potential ligands (Niesen *et al.*, 2007). Significant stabilizing temperature shifts were observed with 5 and 10 mM additions of alpha-ketoglutarate and malate (Table S4). Oxaloacetate only showed a significant positive temperature shift at the highest ligand concentration tested and only in one of the two biological replicates. Additionally, a single trial of isothermal titration calorimetry (ITC) resulted in binding curves, indicating stronger ligand binding with alpha-ketoglutarate, malate and oxaloacetate (K_D values of 25.8, 22.0 55.5 µM respectively), but not succinate or malonate (data not shown). Overall, all three of these binding studies support the binding of the RsbU periplasmic domain to the TCA cycle intermediates alpha-ketoglutarate, malate and oxaloacetate.

Nonsense mutation in rsbU *gene suggests the importance of the Rsb pathway in chlamydial growth*

Based on the three ligands and the potential for the regulation of ATP generation (oxidative phosphorylation), it was hypothesized that the absence of this sensing system could be detrimental to the growth of *Chlamydia*. To evaluate this hypothesis, a *C. trachomatis* L2 EMS mutant (CTL2M401) was obtained (Dr. R. Valdivia; Duke University) that contained an SNP causing a nonsense mutation at W284 in the *ct588* gene coding for the RsbU
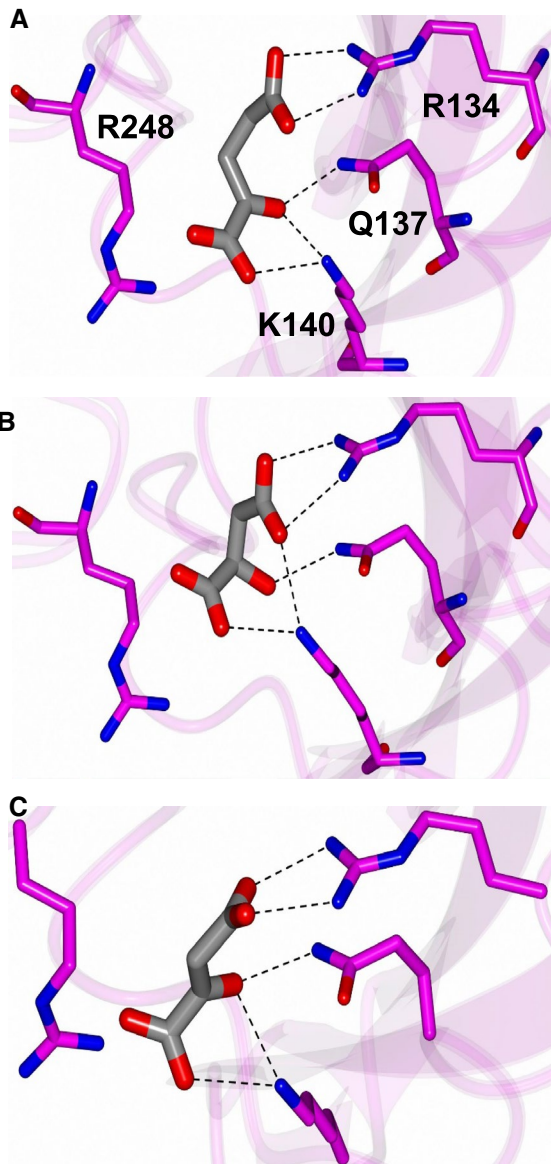
Fig. 6. Ligand docking showing the predicted binding modes of (A) ketoglutarate, (B) malate and (C) oxaloacetate in the binding pocket of RsbU. All the ligands are rendered as gray cylinders. Interacting residues are annotated in panel A.

protein (Nguyen and Valdivia, 2012; Kokes *et al.*, 2015). This nonsense mutation occurs toward the C-terminal end of the periplasmic domain resulting in a truncated protein lacking the cytoplasmic domain. Western blot analysis using antibodies increased against the periplasmic domain supported the absence of the full-length RsbU, as well as any lack of the truncated product, in this mutant strain and is deemed a null mutant (RsbU*; Fig. 7A). Growth of this RsbU* null mutant strain was assessed with DNA harvested at 0, 12, 24, 36, 48 and 72 h postinfection. Genome copy numbers were compared between *Chlamydia* (*secY*) and host (*rpp30*) (Fig. 7B). Striking

differences in the growth pattern of the mutant were observed compared to wild-type *Chlamydia*, with the mutant strain displaying minimal replication capabilities and generation of detectable infectious progeny (Fig. 7B and D).

Whole-genome sequencing of this RsbU* mutant confirmed the truncating SNP in *ct588* (*rsbU*). Thirty-two additional SNPs were also determined (Table S5). Of these SNPs, seven are silent mutations and four are in intergenic regions. The remaining 21 SNPs were evaluated for their potential effect on their respective coding regions with the majority predicted to have no obvious effect on the protein function based on their likelihood to alter secondary structures or active domains as predicted by EMBOSS secondary structure prediction or BLASTp domain predictions. Two SNPs are predicted to alter secondary structures: a G105E mutation in CT259 and a Q204* mutation in CT163. The mutation in CT259 is predicted to form an alpha helix spanning E99 to F113 not predicted in the wild-type CT259 and has been associated with reduced phosphatase activity of the protein (Claywell *et al.*, 2018). The most significant SNP, outside of *rsbU**, is the additional truncation in CT163, a hypothetical protein with no conserved motifs. The CT163 protein is predicted to be a membrane protein with one transmembrane domain in *C. trachomatis*. The truncation stops the translation one-third of the way through the large putative extracellular domain, likely altering protein function. It is unclear what effect the truncation of this protein would have on the chlamydial developmental cycle and we cannot rule out the possibility that the SNP is contributing to the growth and morphological defects that have been determined for the RsbU* null mutant.

To more confidently attribute the growth defect and phenotype to the RsbU disruption rather than the other SNPs induced by EMS mutagenesis, complementation efforts were pursued. However, because of the extremely poor growth of the RsbU* mutant, standard transformation with a wild-type *rsbU* gene on a vector plasmid proved unsuccessful. To overcome this limitation, lateral gene transfer was performed between *C. trachomatis rsbU** (Rif[R]) and another mutant strain that has a transposon (β-lactamase) inserted in *mutL* (*ct575::Tn bla*), which is near the *rsbU* coding region (CT588). After mixed infection and dual antibiotic selection, this was expected to encourage homologous recombination between the two genomes and restore *rsbU* coding region (Fig. S4). This was expected to also leave the majority of SNPs including the *ct163* mutant truncation. Importantly, the transposon mutant strain (*ct575::Tn bla*) showed growth phenotypes matching wild-type *C. trachomatis* L2 strain (Figs 7E and S5).

Sequencing of amplicons from various genomic regions revealed a cross-over region in one of the resulting clones
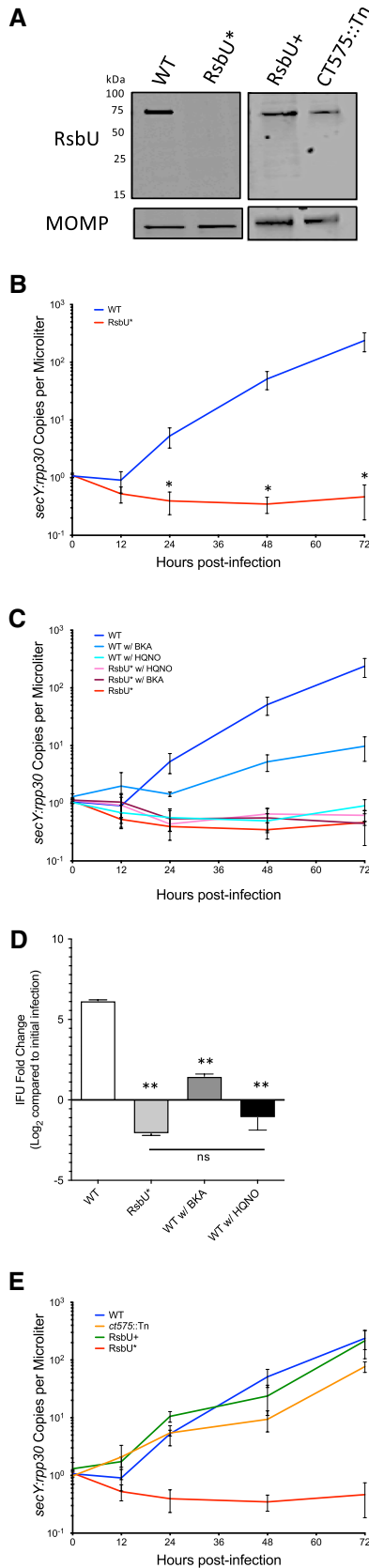
Fig. 7. The Rsb pathway affects the normal growth of *Chlamydia*.
A. Western blot of WT and RsbU* expression of RsbU protein at 24 h postinfection. No RsbU protein fragment is detected in the RsbU* mutant strain. MOMP is used as a loading control.
B. *Chlamydia* genome copy numbers (*secY*) were compared to host cell genome copy numbers (*rpp30*) over 72 h after the initial infection. RsbU* appears to begin replicating around 72 h postinfection (*P-value < 0.05 with student's T-test).
C. Growth curves with chemical inhibitors, HQNO and BKA show significant differences between WT and WT +BKA after 24 h, as well as RsbU* and WT + BKA (P-value > 0.05). With HQNO added, both WT and RsbU* were not statistically different from RsbU* without any inhibitors.
D. Progeny assay looking at the difference in IFUs produced after 36 hpi compared to the IFUs in the initial infection. The decrease in IFUs produced by the RsbU* strain, as well as WT treated with HQNO, suggest that the chlamydial cells are largely in the RB form at this point in the infection rather than the EB form capable of propagating the infection to new host cells. While all three experimental conditions were significantly different from the WT untreated condition (**P-value < 0.001 with student's T-test), the RsbU* mutant compared to the HQNO-treated infection shows no significant difference (P-value = 0.3).
E. The RsbU+ recombinant strain, with WT RsbU expression but retaining the majority of the other EMS-induced SMPs, restores growth to WT levels.

obtained following mixed infection and dual selection. Upon whole-genome sequencing this complemented strain, the RsbU+ strain was revealed to be a mosaic between the RsbU* and wild-type genomes with a couple of different regions of recombination apparent. In addition to a wild-type *rsbU* gene, the RsbU+ strain also has wild-type versions at 14 of the 32 SNP loci, 11 of which are in coding regions (Fig. S4). Because the complemented strain does not retain all of the RsbU* SNPS, it does leave open the possibility that one or more of those SNPs could be playing a role in the growth defect of the null mutant that is restored in the complemented strain. In particular, the SNP in the *rpoD* gene encoding σ^{66} could affect the growth of the organism; however, the position of the SNP does not suggest a change in the structure of the protein and exists in a region of the protein with no apparent DNA-binding interaction (Paget, 2015). Importantly, however, in the RsbU+ complemented strain, the nonsense mutation in the *ct163* gene is maintained, meaning that any growth difference between the mutant and complemented strain is not due to this mutation. Growth curves were done with the parental transposon strain and the RsbU+ complemented strain, revealing that the RsbU+ strain showed a restoration in the growth rate (Fig. 7E).

We then hypothesized that the binding of TCA cycle intermediates to RsbU could indicate that the Rsb pathway is playing a regulatory role on TCA cycle activation in the chlamydial developmental cycle, leading to poor growth of the RsbU* mutant. To test this hypothesis, we looked into chemical inhibitors targeting *Chlamydia*'s ability to produce ATP itself, as well as to steal ATP from the

host cell using ATP translocases. 2-heptyl-4-hydroxyquinoline N-oxide (HQNO) has been shown at low concentrations (1µM) to selectively inhibit the sodium-dependent NADH dehydrogenase that *Chlamydia* utilizes to produce the ion gradient that drives ATP synthesis by the chlamydial ATP synthase (Tuz *et al.*, 2015; Liang *et al.*, 2018). Alternatively, bongkrekic acid (BKA) has been shown to inhibit ATP translocases in *Chlamydia,* limiting the ability to utilize host ATP (Winkler and Neuhaus, 1999). Growth curves were repeated with wild-type *Chlamydia* and the RsbU* mutant strain with the addition of the chemical inhibitors (Fig. 7C). BKA caused a decrease in the growth of wild-type *Chlamydia* that is statistically significant from wild-type (*P*-value < 0.05) after 24 h, as well as from the RsbU* mutant after 24 h. The addition of HQNO to a wild-type infection, however, was not statistically different from the RsbU* mutant growth at any time point.

Additionally, progeny production was assessed for the RsbU* mutant strain, as well as wild-type infections, with the BKA and HQNO chemical inhibitors (Fig. 7D). This assay revealed that, while there is a decrease in IFUs produced in the presence of BKA compared to the untreated WT infection, viable EBs are still being produced. However, in the RsbU* and WT + HQNO conditions, there is a decrease in the number of IFUs produced compared to the initial infection, suggesting that these cells are in the RB noninfectious form rather than converting to the infectious EB form. This is consistent with the growth curves in Fig. 7C where genome copies can be detected for these conditions, but RB-to-EB conversion appear to stalled in the infection.

To further investigate the poor growth by the wild-type *Chlamydia* in the presence of the sodium-dependent NADH dehydrogenase inhibitor (HQNO) and translocase inhibitor (BKA) as well as by RsbU*, confocal microscopy was carried out to view L929 cells infected with wild-type *Chlamydia* or RsbU* with and without inhibitors at 24 and 72 h (Fig. 8). Image analysis revealed that the wild-type *Chlamydia* at 24 h postinfection in the presence of HQNO inhibitor formed smaller inclusions and appear to contain fewer EBs (puncta), although chlamydial RB cells appear like wild-type. At 72 h postinfection, *Chlamydia* infected in the presence of HQNO had inclusions that were considerably smaller compared to wild-type *Chlamydia* with no inhibitor. No obvious morphological abnormalities were apparent for wild-type *Chlamydia* in the presence of the BKA inhibitor. RsbU* was shown to have a severe growth defect with no defined development of inclusion. Additionally, *Chlamydia* cells appear dispersed in the host cytosol and far fewer than those levels observed by wild-type *Chlamydia* at both 24 and 72 h postinfection. RsbU* mutant infections at both 24pi do appear to contain both EB and RB *Chlamydia* cell forms. The addition
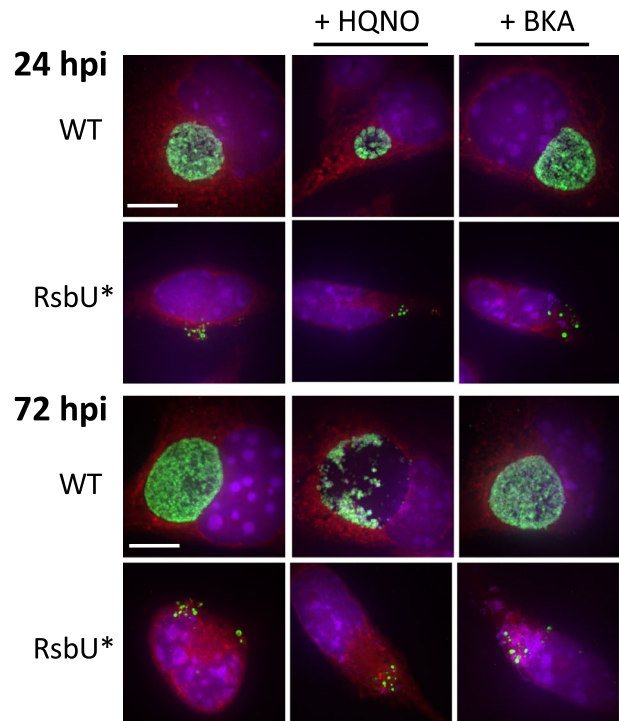

Fig. 8. Immunofluorescent microscopy of *Chlamydia* with RsbU* disruption and inhibitors of sodium-dependent NADH dehydrogenase and ATP translocase. L929 cells infected with wild-type *Chlamydia trachomatis* or RsbU* with and without the presence of inhibitor (HQNO or BKA) at 24 and 72 h postinfection. Blue: DAPI, nucleus; Red: Evan's Blue, cytoplasm; Green: OmpA, *C. trachomatis* organisms. Images were acquired by confocal microscopy using a 150X objective and are comprised of seven compressed *Z*-stacks (maximum projection) for each field.

of the HQNO and BKA inhibitors appeared to have no effect on levels of RsbU* C*hlamydia* or their dispersion within the host cell.

Overall, growth with HQNO causes a marked reduction in growth in wild-type chlamydial infections, but does not have an additive effect on the growth defect observed in the RsbU* mutant. These observations support that the Rsb pathway in *Chlamydia* is linked to the ability of the bacteria to generate ATP via oxidative phosphorylation.

Transcriptional analysis of TCA cycle-associated and constitutively active genes suggestive of the Rsb pathway regulation of σ⁶⁶ activity

σ^{66} is the primary sigma factor of only three sigma factors that *Chlamydia* sp. possess and is responsible for the transcription of the vast majority of genes throughout the developmental cycle. In order to further explore the proposed link between the Rsb pathway in *Chlamydia* to the regulation of σ^{66} (Thompson *et al.*, 2015), transcript levels of σ^{66}-transcribed genes were assessed for differential expression between the RsbU* mutant and WT L2 *C. trachomatis*
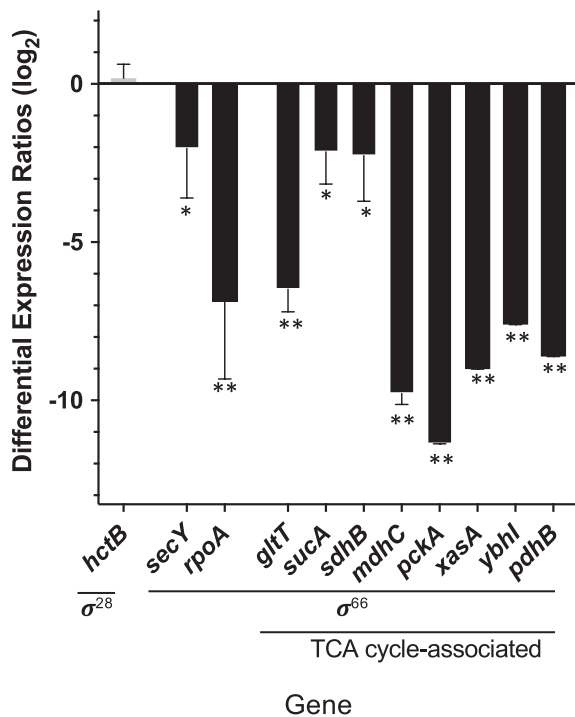
Fig. 9. Differential expression of TCA cycle-associated genes and other sigma-66 transcribed genes in RsbU* mutant compared to WT L2 transcript levels at 24 hpi. Genomic levels of DNA per infection were used to normalize transcript counts. Sigma-28 transcribed gene, *hctB,* shows similar transcript levels between the RsbU* mutant and WT L2, while those genes with σ^{66} promoters all show significant decreases in the level of transcripts (*P-value > 0.05; **P-value > 0.01 with student's *T*-test). Genes selected for this analysis included TCA cycle-associated genes (*gltT, sucA, sdhB, mdhC, pckA),* constitutively active genes (*secY, rpoA, dnaK)* and other genes associated with dicarboxylate processing or transport (*xasA, ybhI, pdhB),* all of which as σ^{66}-transcribed genes.

(Fig. 9). Genes chosen for this analysis included TCA cycle-associated genes (*gltT, sucA, sdhB, mdhC, pckA*), constitutively active 'housekeeping' genes, (*secY, rpoA, dnaK*) and other genes associated with dicarboxylate processing or transport (*xasA, ybhI, pdhB*) (Iliffe-Lee and McClarty, 2000). All σ^{66}-transcribed genes were observed to have lower transcript counts compared to wild-type, while the σ^{28}-transcribed gene *hctB*, did not appear to be differentially expression between the two strains. These results suggest that when the Rsb pathway is disrupted, as in the RsbU* mutant strain, there is a decrease in the transcription of these genes under the regulation of the σ^{66} activity.

Discussion

To characterize the role of the Rsb phosphoregulatory partner-switching pathway in *Chlamydia*, we focused on the structure and ligand-binding capabilities of the periplasmic domain of RsbU. A 1.7 Å crystal structure for the periplasmic domain (Fig. 3) allowed for structural

comparisons to other proteins, leading to the identification of a putative binding pocket and a possible association to the native ligand.

SPR (Table 1 and Fig. S3), DSF (Table S4) and ITC (data not shown) experiments suggest that alpha-keto-glutarate, malate and oxaloacetate are binding to RsbU$_{45\text{-}313}$. Dose-dependent SPR binding studies allowed for the calculation of an estimated K_D value of 419, 459 and 396 μM for alpha-ketoglutarate, malate and oxalo-acetate respectively. This is a relatively high K_D value, indicative of weak binding, however, the concentrations of alpha-ketoglutarate and malate used were those similar to physiological levels in the cell (Albe *et al*., 1990). Similar proteins including Tlp3 from *Campylobacter jejuni* and PctA, PctB and PctC from *Pseudomonas aeruginosa* have been shown to bind ligands at similar binding affinities (Rico-Jimenez *et al*., 2013; Rahman *et al*., 2014). Alternatively, there are several factors that could be having an effect on the RsbU$_{45\text{-}313}$ protein's ability to bind to the ligand, including the need for dimerization for ligand binding and the lack of the cytoplasmic and trans-membrane portions of the protein that help to stabilize the protein binding (Delumeau *et al*., 2004; Zhou *et al*., 2008; Nan *et al*., 2010; Liu *et al*., 2015). The K_D values from the single ITC experiment were about a log lower than those values calculated from SPR, indicating stronger binding affinity. This discrepancy is due to the difference in the condition of the protein (free in solution with ITC compared to cross-linked to a surface with SPR). The K_D values from the ITC experiment are closer to the K_D determined for DctB binding to succinate, also determined by ITC (Nan *et al*., 2010).

The binding of multiple ligands allows for the possibility of differential responses upon binding. DctB has been shown to bind to both succinate and malonate, with a conformational change and loop closure of 2.2 Å with succinate, but not with malonate binding (Zhou *et al*., 2008). The aforementioned structurally similar Tlp3 and Pct proteins also have been shown to bind to multiple ligands and have differential responses based on the identity of the ligand (Rico-Jimenez *et al*., 2013; Rahman *et al*., 2014).

Determining that RsbU is binding to TCA cycle intermediates lends itself to the question of what role this protein and its related pathway are playing in the chlamydial developmental cycle. To investigate the effect of RsbU on chlamydial growth, an RsbU* mutant showed a severe deficit in growth compared to the wild-type strain supporting that the Rsb pathway plays a role in the normal pattern of chlamydial growth (Fig. 7B) (Kokes *et al*., 2015). When complementation of the *rsbU* gene was accomplished through homologous recombination with the *ct575*::Tn strain, the growth pattern returned to wild-type-like levels (Fig. 7E).

Chlamydia has different ways that it can acquire energy. The presence of two ATP-ADP translocases allows for ATP uptake from the host cell appears to be the main source of energy when in the early stages of the developmental cycle, immediately after entry into the cell (Tjaden *et al.*, 1999). *Chlamydia* is then able to manufacture its own ATP utilizing a sodium-ion gradient to drive its ATP synthase activity during RB replication in mid-cycle time points as demonstrated by a recent publication by Liang *et al.* (2018). Wild-type chlamydial growth with HQNO, a sodium-dependent NADH dehydrogenase inhibitor, appears to mimic the growth pattern of the RsbU* mutation, potentially stalling the RB-to-EB conversion reducing the number of infectious progeny in the late stage of the developmental cycle as well (Fig. 7C and D). While it is possible that the loss of the NADH-driven sodium gradient might also impact other processes that utilize the ion gradient, such as amino acid transport, when RsbU* was grown in the presence of HQNO, the growth pattern was similar to that of wild-type with HQNO. These data suggest that the inhibition of the sodium-dependent NADH dehydrogenase in the RsbU* strain does not have an additive effect on the growth defect and that the Rsb pathway may be playing a role in the *Chlamydia*'s production of ATP through oxidative phosphorylation.

The dynamic energy utilization could account for the nonlethality of the RsbU* mutation. If *Chlamydia* is able to actively scavenge ATP and other metabolites from the host in its early developmental cycle, then there is a possibility of replication as well, albeit much more slowly. Moreover, there is a possibility of redundant pathways for the activation of metabolic and replicative machinery. A second antagonist to the RsbW protein, $RsbV_2$ (CT765), is also present in *Chlamydia.* Previous studies have shown that RsbU only dephosphorylated $RsbV_1$, while RsbW phosphorylated both RsbV proteins, but has a bias toward $RsbV_1$ (Hua *et al.*, 2006; Thompson *et al.*, 2015). The duality of RsbW antagonists could potentially mean that there is a secondary signal that has a similar, but possibly lesser, effect on the repression of RsbW inhibition of the downstream target protein, and thus why the RsbU signaling disruption is not lethal.

The target protein(s) for RsbW in *Chlamydia* is debatable. Several studies have investigated the potential protein interaction partners of RsbW to identify its target protein. Based on the Rsb system in *B. subtilis,* the target is presumed to be a sigma factor, for which *Chlamydia* has only three (Wise and Price, 1995). However, conflicting results have been observed in interaction studies with the primary chlamydial sigma factor, σ^{66}, in addition to the alternative sigma factors, σ^{28} and σ^{54}. Douglas and Hatch demonstrated that RsbW pulled down with σ^{28} *in vitro*, while Hua and colleagues found that RsbW did not interact with any of the chlamydial sigma factors using a yeast two-hybrid

system and an *in vitro* σ^{28}-dependent transcription assay (Douglas and Hatch, 2000; Hua *et al.*, 2006). Most recently, Thompson *et al.* found using a bacterial two-hybrid system, and validated using SPR experiments, that RsbW binds σ^{66}, but not σ^{54} or σ^{28} (Thompson *et al.*, 2015). These data have led to some uncertainty for any one sigma factor as the target protein, and the possibility for a nonsigma factor target has yet to be fully investigated. While the Rsb pathway described in *B. subtilis* and other gram-positive bacteria regulates an alternative sigma factor, it is also worth considering that this pathway in *Chlamydia* may not be regulating such transcriptional machinery. In *Bordetella*, an RsbU homolog has been shown to be an important regulator of the type III effector protein secretion without affecting transcription (Mattoo *et al.*, 2004; Kozak *et al.*, 2005). Further efforts are being made to more definitively determine the target protein of the Rsb pathway and its specific role in the chlamydial developmental cycle; however, in this study, the differential expression of σ^{66}-transcribed genes, TCA cycle-associated and otherwise, was also assessed (Fig. 9). Of the genes selected for the transcriptional analysis, all σ^{66}-transcribed genes appear to be down-regulated in the RsbU* mutant compared to WT L2 *C. trachomatis,* in contrast to σ^{28}-transcribed *hctB* (Yu and Tan, 2003). This differential expression pattern between the RsbU* mutant and wild-type *Chlamydia* shows a correlation between a disruption in the Rsb pathway and a decrease in σ^{66}-transcribed gene transcript levels.

If the Rsb pathway regulates σ^{66}, as the most recent publication and this study suggests (Thompson *et al.*, 2015), the binding of alpha-ketoglutarate seems rational. *Chlamydia* is known to obtain alpha-ketoglutarate from the host cell as a means for fueling its truncated TCA cycle to produce ATP through oxidative phosphorylation (Iliffe-Lee and McClarty, 2000). The presence of a pool of alpha-ketoglutarate that *Chlamydia* can access could be an indicator that the bacteria is inside of the host cell and in a favorable environment for replication, and thus the activation of the primary sigma factor. The regulation of σ^{66} by the Rsb pathway may also explain the difference in the morphology of the RsbU* mutant compared to the wild-type *Chlamydia* with the HQNO inhibitor. While the HQNO inhibitor in the wild-type infection does mimic the RsbU* growth pattern, the IFA imaging (Fig. 8) is not an exact phenocopy. There is still an obvious inclusion present in the wild-type infection in the presence of HQNO, although the amount of *Chlamydia* is clearly less, compared to the RsbU* mutant which does not appear to be inside of inclusion, but instead clustered together in the host cell cytoplasm. The wild-type infection, in this case, would still have the ability to activate σ^{66}, while the RsbU* would have σ^{66} repression, thus having a larger pleiotropic effect and be diminished in its ability to transcribe genes for the establishment and maintenance of the inclusion,

TCA cycle enzymes, and effective growth and replication of the organism. Liang *et al.* were also able to show similar growth phenotype when wild-type *Chlamydia* is in the presence of monensin, a Na^+/H^+ exchanger that dissociates the Na^+ ion gradient driving the chlamydial ATP synthase (Liang *et al.*, 2018).

The idea of dynamic energy utility also leads to our proposed model of how the Rsb partner-switching pathway is playing a role in the *Chlamydia* developmental cycle (Fig. 10). When an EB enters the host cell it comes in contact with an increased level of alpha-ketoglutarate, which binds to the RsbU periplasmic domain. In the current model, upon binding to alpha-ketoglutarate, the cytoplasmic effector domain of RsbU performs its phosphatase activity on $RsbV_1$. RsbW then releases its target protein to rephosphorylate the $RsbV_1$ protein. That target protein then affects the activation of the TCA cycle in *Chlamydia.* This effect could be indirect, being a sigma factor, such as σ^{66}, or through the other transcriptional regulators or machinery that lead to the expression of other proteins involved in the TCA cycle; or direct, through the activation of transport proteins for TCA cycle substrates or enzymes in the TCA cycle itself. Then when levels of alpha-ketoglutarate are waning, potentially toward the end of the developmental cycle, RsbU is no longer bound and the target protein is again inhibited by RsbW. Interestingly, temperature-sensitive mutants generated by Brothwell *et al.* for both *sodTi* (the putative dicarboxylate transporter) and *gltT* (the putative glutamate transporter) support that the acquisition of alpha-ketoglutarate is important for chlamydial growth (Brothwell *et al.*, 2016). In addition, the

levels of malate and/or oxaloacetate in the periplasm could act as an inhibitor for RsbU signaling. Malate or oxaloacetate could build up in the periplasm as it is transported out of the chlamydial cytoplasm by transporter proteins such as SodTi (Weber *et al.*, 1995). The phosphoenolpyruvate carboxylkinase (Pck) enzyme catalyzing the conversion of oxaloacetate to phosphoenolpyruvate has been shown to be differentially regulated as a mid-late stage gene, possibly leading to more malate and oxaloacetate being present in the cytoplasm to be exported into the periplasm by SodTi in exchange for alpha-ketoglutarate (Belland *et al.*, 2003; Nicholson *et al.*, 2003). Additionally, malate converted to oxaloacetate can also be used to synthesize *meso*-diaminopimelate (mDAP), a cross-linker in the A1γ-type peptidoglycan *Chlamydia* synthesizes during growth (Pilhofer *et al.*, 2013; Packiam *et al.*, 2015). Peptidoglycan is only needed during the growth of the *Chlamydia* cell (Liechti *et al.*, 2014; Packiam *et al.*, 2015), and therefore a buildup of malate could occur as the cell ceases the growth in preparation for the conversion to the EB form.

Aspects of the Rsb phosphoregulatory partner-switching pathway remain to be explored. While the transcriptional analysis supports the hypothesis that the target protein of the pathway could be σ^{66}, it does leave open the possibility of RsbW binding to a secondary transcriptional regulator. A phosphoproteomic analysis performed in *Chlamydia caviae* showed that phosphorylated $RsbV_1$ and $RsbV_2$ can be detected in EBs, but not in RBs, rather than the other way around; calling into question the nature of this intermediate connection between RsbU and RsbW, and the mechanism
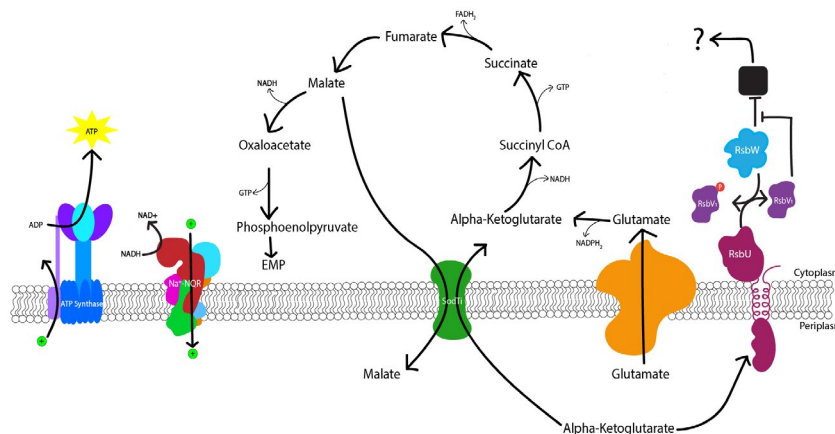
Fig. 10. Working model of the Rsb phospho-regulatory pathway integrated with the truncated TCA cycle in *Chlamydia.* Alpha-ketoglutarate binding to the periplasmic domain of RsbU, as could be the case when an EB enters the host cell, leads to the activation of the phosphatase function of the cytoplasmic domain. RsbW then releases its target protein (black box), allowing for its normal function to be performed. That target protein then, either directly or indirectly, activates the chlamydial TCA cycle, allowing for alpha-ketoglutarate to be utilized. *Chlamydia* has been shown to be capable of creating its own ATP during mid-cycle using a truncated TCA cycle to generate electron-carrying molecules (i.e. NADH, $FADH_2$) and a sodium pumping NADH:quinone oxidoreductase (Na^+-NQR) (Liang *et al.*, 2018). As malate builds up in the periplasm, through the export by the SodTi protein (Weber *et al.*, 1995), it acts as an inhibitor as the concentration of alpha-ketoglutarate is depleted. The inhibition of the RsbU protein or the depletion of alpha-ketoglutarate, potentially later in the developmental cycle, could lead to a slowing of the TCA cycle as the *Chlamydia* cells prepare to convert to the EB form.

of which these proteins communicate (Fisher *et al.*, 2015). Furthermore, the true response of RsbU to binding either alpha-ketoglutarate, malate or oxaloacetate; whether they are activating or inhibiting the phosphatase activity of the RsbU cytoplasmic domain, still remains to be fully examined.

In this study, we were able to solve a 1.7 Å crystal structure for the periplasmic domain of the chlamydial RsbU protein and utilize structural similarities to a dicarboxylate-binding protein to determine alpha-ketoglutarate, malate and oxaloacetate as binding ligands. Moreover, an RsbU null mutant was utilized to show the importance of the Rsb pathway in normal chlamydial growth. Finally, we proposed a working model for how this pathway may be sensing the aforementioned ligands to regulate the TCA cycle.

Experimental procedures

Overexpression and purification of recombinant RsbU$_{45-313}$

A fragment of *ctl0851* encoding residues 45 through 313 of the open reading frame was amplified via polymerase chain reaction (PCR) from *C. trachomatis* L2 434/Bu (AM884176) genomic DNA. *ctl0851* is homologous and 99% identical to CT588 (RsbU) from *C. trachomatis* D/UW-3. This fragment was inserted into the pTBSG vector in the frame and immediately downstream of a sequence encoding an N-terminal hexahistidine tag and TEV protease recognition site. After confirming sequence, this vector was transformed into BL21 (DE3) *Escherichia coli* competent cells, which were then grown at 37°C (200 rpm) in Terrific Broth supplemented with 100 μg ml^{-1} Carbenicillin to an OD$_{600}$ of 0.8. Overnight protein expression (15°C, 200 rpm) was induced at this optical density with the addition of IPTG (isopropyl 1-thio-β-D-galactopyranoside) to a final concentration of 1 mM. Following *E. coli* collection by centrifugation (10,000*g*; 15 min), cells were resuspended in lysis buffer [20 mM Tris pH 8.0, 500 mM NaCl, 10 mM imidazole, 1 mM phenylmethane sulfonyl fluoride (PMSF) and 1000U Benzonase endonuclease (EMD Millipore) per liter of Terrific broth culture] and lysed by sonication. After centrifugation (23,000*g*; 30 min), the supernatant was clarified through a 0.45 μm filter and purified on a gravity flow column containing 3 mL of HisPur Cobalt Resin (Thermo Fisher) per liter of Terrific Broth culture. Following washes with five column volumes (CVs) of lysis buffer and then three CVs of wash buffer (20 mM Tris pH 8.0, 500 mM NaCl and 50 mM imidazole), immobilized His$_6$-RsbU$_{45-313}$ was eluted with three CVs of elution buffer (20 mM Tris pH 8.0, 500 mM NaCl and 500 mM imidazole). The eluate was buffer exchanged into Buffer A (20 mM Tris pH 8.0, 500 mM NaCl and 10 mM imidazole) on a HiPrep 26/10 Desalting column (GE Healthcare) and then incubated overnight at 4°C with 5 mM dithiothreitol (DTT) and recombinant polyhistidine-tagged TEV protease for His$_6$-tag removal. Recombinant TEV protease and cleaved His$_6$-tag were then removed from this mixture via flow over a 5 mL HisTrap HP column (GE Healthcare). Following buffer exchange into Buffer X (10 mM Tris pH 7.5, 50 mM NaCl, and 1 mM DTT) as described above, the sample was concentrated to a volume of 1.5 mL with an Amicon-15, Ultracel-10 centrifugal filter (EMD Millipore). Final purification was achieved via size exclusion chromatography using a flow rate of 0.2 ml min^{-1} on a HiPrep 16/60 Sephacryl S-200 HR column (GE Healthcare). Collected fractions containing RsbU$_{45-313}$ were concentrated to 15.9 mg ml^{-1} (by Bradford assay) via ultracentrifugation and stored at 4°C until further use.

Crystallization and data collection

All crystallization screening was conducted in Compact 300 (Rigaku Reagents) sitting drop vapor diffusion plates at 18°C using equal volumes of protein solution and crystallization solution equilibrated against 75 μl of the latter. Prismatic crystals grew within one day and continued to grow for approximately one week from Wizard 1-2 screen (Rigaku Reagents) condition E10 (1 M ammonium phosphate dibasic, 100 mM Tris pH 8.5) and the Crystal Screen HT (Hampton Research) condition D5 [20% (w/v) PEG 4000, 10% (v/v) 2-propanol, 100 mM HEPES pH7.5]. A heavy atom derivative was prepared by soaking a crystal obtained from Wizard 1-2 condition E10 for 22 h in crystallant containing 5 mM K$_2$PtCl$_4$. Native and heavy atom-soaked crystals were transferred to a fresh drop containing 80% crystallant and 20% ethylene glycol before flash freezing in liquid nitrogen. Data were collected at the Advanced Photon Source IMCA-CAT beamline 17-ID using a Dectris Pilatus 6M pixel array detector.

Structure solution and refinement

Intensities were integrated using XDS via Autoproc, and the Laue class analysis and data scaling were performed with Aimless (Kabsch and Sander, 1983; Evans, 2011; Vonrhein *et al.*, 2011). The highest probability Laue class was *4/m*, for either space group *I4* or *I4$_1$*. The Matthew's coefficient (Vm) and solvent content were estimated to be Vm = 2.3/47% solvent for one molecule in the asymmetric unit (Matthews, 1968). Data for phasing were collected using the platinum-soaked crystals, at the absorption edge λ = 1.0716 Å (11.570 keV) as determined from an X-ray fluorescence scan. Integrated diffraction data from two crystals were scaled together with Aimless to increase the multiplicity. Structure solution was conducted using the SAD method with Autosolve via the Phenix interface, which yielded a figure of merit of 0.23 and a Bayes-CC of 0.299 (Adams *et al.*, 2010). The Autobuild step of Autosolve produced a model containing 188 of the possible 272 residues which converged at R = 0.35, R$_{free}$ = 0.44 following refinement. Crystals of native RsbU obtained from the Crystal Screen HT condition D5 yielded the highest resolution diffraction (1.7 Å) and were used from this point forward. The resulting model from Autosolve was used for molecular replacement with Phaser against a native RsbU data set and the top solution was obtained in the space group *I4* (TFZ = 45.8, LLG = 1,836) (McCoy *et al.*, 2007). The model was further improved by the automated model

Table 2. X-ray diffraction data and structure refinement.

	RsbU (K2PtCl4)	RsbU (Native)
Data collection		
Cell dimensions		
a, b, c (Å)	96.71, 96.71, 96.49	96.71, 96.71, 96.39
α, β, γ (°)	90.00, 90.00, 90.00	90.00, 90.00, 90.00
Space group	I4	I4
Resolution (Å)[a]	48.36–2.30 (8.91–2.30)	48.36–1.70 (1.73–1.70)
Wavelength (Å)	1.0716	1
Temperature (K)	100	100
Observed reflections	352,983 (33,886)	225,529 (11,050)
Unique reflections	13,526 (1,297)	33,233 (1,758)
$<I/\sigma(I)>$[a]	18.5 (1.7)	17.9 (1.7)
Completeness (%)[a]	100.0 (100.0)	100.0 (100.0)
Multiplicity	26.1 (26.1)	6.8 (6.3)
R_{merge} (%)[a,b]	11.5 (119.6)	6.1 (111.0)
R_{meas} (%)[a,c]	11.7 (122.0)	6.6 (121.1)
R_{pim} (%)[a,c]	2.3 (23.9)	2.5 (47.8)
Refinement		
Resolution (Å)		36.07 - 1.70
Reflections (working/test)		33,231 (3,266)
R_{factor}/R_{free} (%)[d]		16.36/19.73
No. of atoms (protein/ligand/water)		2,101/1/203
Model quality		
R.m.s. deviations		
Bond length (Å)		0.008
Bond angles (°)		0.914
Average *B* factor (Å)		
All Atoms		23.11
Coordinate error, maximum likelihood (Å)		0.19
Ramachandran plot		
Most favored (%)		98.11
Additionally allowed (%)		1.89

[a]Values in parentheses are for the highest resolution shell.

[b]$R_{merge} = S_{hkl}S_i \,|I_i(hkl) - <I(hkl)>| \,/\, S_{hkl}S_i \,I_i(hkl)$, where $I_i(hkl)$ is the intensity measured for the ith reflection and $<I(hkl)>$ is the average intensity of all reflections with indices hkl.

[c]R_{meas} = redundancy-independent (multiplicity-weighted) R_{merge} (Diederichs, 1997; Evans, 2011). R_{pim} = precision-indicating (multiplicity-weighted) R_{merge} (Weiss, 2001; Evans, 2006).

[d]$R_{factor} = S_{hkl} \,||F_{obs}(hkl)| - |F_{calc}(hkl)||\,/\,S_{hkl} \,|F_{obs}(hkl)|$; R_{free} is calculated in an identical manner using 5% of randomly selected reflections that were not included in the refinement.

building using Arp/wARP and subsequent rounds of structure refinement and manual model building were carried out using Phenix and Coot (Langer *et al.*, 2008; Emsley *et al.*, 2010). Residues P162, L163 and R313 were not modeled due to inadequate electron density. TLS refinement was incorporated in later rounds to model anisotropic atomic displacement parameters (Winn *et al.*, 2001; Painter and Merritt, 2006). Structure validation was conducted with Molprobity and relevant crystallographic data are provided in Table 2 (Chen *et al.*, 2010). Coordinates and structure factors for RsbU were deposited in the Worldwide Protein Databank (wwPDB) with the accession code 6MAB.

Structural alignments and superimposition

Structures of DctB were obtained from the PDB. Apo DctB (3E4Q), malonate-bound DctB (3E4P), and apo RsbU were aligned to beta-sheet residues (120–198) of succinate-bound DctB (3E4O) using the combinatorial extension alignment method (O'Hearn *et al.*, 2003). Alignments were performed using the NCBI Blast webserver (Coordinators, 2017). Global

alignments were performed using the Needleman-Wunsch method and local alignments were performed using BLAST. Proteins with the same fold were identified by performing a TM-alignment (Zhang and Skolnick, 2005) of RsbU against the nonredundant structures from the PDB (Yang *et al.*, 2015). Proteins that had a TM-score of at least 0.5, when normalized against RsbU, were considered to have the same fold (Zhang and Skolnick, 2004; Xu *et al.*, 2010).

Virtual screen of human metabolite and chlamydial metabolite libraries

The human metabolites set of compounds were downloaded from the Human Metabolite Database and compounds with a molecular weight greater than 300 were discarded (Wishart *et al.*, 2007, 2009, 2018). The *Chlamydia* metabolites set of compounds were downloaded from the *C. trachomatis* database in BioCyc (Caspi *et al.*, 2016). Up to 250 conformers were generated using Omega (version 2.5.1.4) by OpenEye (Santa Fe, NM) (Hawkins *et al.*, 2010). The receptor was prepared using

APOPDB2RECEPTOR and compounds were docked into using FRED (version 3.2.0.2) at the 'Standard' docking resolution (Santa Fe, NM), (McGann, 2011). Docked models were refined using SZYBKI (version 1.9.0.3) (Sant Fe, NM). Compounds with docking scores above –6 (chosen based on the docking score of succinate), positive interaction energies and minimized ligand poses that moved more than 1.5 Å were discarded. The remaining compounds were enriched with malate, malonate, alpha-ketoglutarate, succinate, α-D-glucose, fumarate, glutamate, pyruvate, 3-phosphoglyceric acid, oxaloacetate and aldohexose stereoisomers. Compounds were prepared using LigPrep by Schrodinger using the default settings (New York, NY) to identify the physiologically relevant protonation states. The receptor was prepared using the protein preparation wizard in Schrodinger, which optimizes the hydrogen bonding and protonation state, followed by a constrained minimization. These compounds were then docked into the receptor using Glide (release 2017-3) by Schrodinger. Up to five docked poses were generated per compound, using extra precision (XP) settings (Friesner *et al.*, 2004, 2006; Halgren *et al.*, 2004). Docked poses were then refined and free energies of binding were predicted using Prime MM-GBSA, allowing the flexibility in residues within 8 Å of the ligand (Jacobson *et al.*, 2002, 2004). Compounds were selected based on the docking score, MM-GBSA predicted energy, predicted ligand efficiency and visual inspection of the models.

The docking models of oxaloacetate, alpha-ketoglutarate and malate to RsbU were generated by docking using Glide XP followed by Prime MM-GBSA refinement, allowing flexibility in residues within 8 Å of the ligand.

Surface plasmon resonance

SPR analyses were performed on a Biacore T200 (GE Healthcare Life Sciences) with cell culture grade Phosphate Buffered Saline (Corning). Purified $RsbU_{45-313}$ protein in PBS was immobilized onto a Series S NTA or CM5 sensor chip (GE Healthcare Life Sciences). All ligands were dissolved in PBS and PBS only was used as a negative control. A flow cell with no protein bound was used as a reference cell for all runs. Ligands were injected over the chip for 30 s, with a 60 s dissociation period. Binding affinity was manually estimated using the steady-state affinity equation:

$$R_{eq} = \frac{CR_{max}}{K_D + C}$$

where R_{eq} is the measured resonance units at steady-state binding levels, C is the concentration of the ligand and R_{max} is the maximum binding capacity determined for each respective ligand assuming a 1:1 ratio of binding to protein.

Data were analyzed using Biacore T200 software (version 3.0).

Differential scanning fluorimetry

$RsbU_{45-313}$ was purified as described above and buffer exchanged into PBS (Corning). DSF was performed with SYPRO Orange (Invitrogen) in a 384-well plate (Roche) format (Niesen *et al.*, 2007). The following potential ligands were tested: succinate, malonate, glutamate, alpha-ketoglutarate, fumarate, oxaloacetate, malate, 2-phosphoglycerate, glucose, pyruvate, phosphoenolpyruvate and ATP (Sigma-Aldrich). All ligands were dissolved in PBS. Compounds were added to each well, followed by DSF buffer HEPES-NaOH pH 7.5 (100 mM), and a 10X SYPRO Orange dye. Reliable baselines for Tm shifts were established using 10X SYPRO Orange and 10 μM $RsbU_{45-313}$. The mixture was heated from 20 to 85°C. Melting curves were analyzed on Roche Tm Analysis software.

Isothermal titration calorimetry

$RsbU_{45-313}$ (30 μM) was purified as described above and buffer exchanged into PBS (Corning). Alpha-ketoglutarate, malate, oxaloacetate, malonate and succinate (Sigma-Aldrich) were dissolved in the same PBS used for the buffer exchange of the $RsbU_{45-313}$ protein at a concentration of 30 mM. ITC was performed on a MicroCal PEAQ-ITC (Malvern Panalytical and analyzed using MicroCal ITC Analysis software (version 1.21).

Growth curves

An EMS mutant strain of *C. trachomatis* L2 was obtained from the Valdivia lab at the Duke University Medical Center (Nguyen and Valdivia, 2012; Kokes *et al.*, 2015). A confluent monolayer of L929 mouse fibroblast cells was infected with an MOI of 0.5 mutant or wild-type chlamydial cells with centrifugation and using Hanks' balanced salt solution with calcium and magnesium (Corning). After centrifugation, the HBSS was removed from the cells and replaced with RPMI (Corning) supplemented with 5% FBS (Millipore), 10 μg ml^{-1} gentamycin and 1 μg ml^{-1} cycloheximide. For the growth curves with the addition of chemical inhibitors, the BKA and HQNO were added into the RPMI at the time of infection. HQNO was added at a final concentration of 1 μM. BKA was added at a final concentration of 0.25 μM. The infected cells were incubated at 37°C, 5% CO_2 until harvested. Total DNA was harvested from infected cells at 0, 12, 24, 36, 48 and 72 h postinfection. DNA was harvested by adding 200 μl of 5 mM DTT, 200 μl of Buffer AL from a Blood and Tissue Kit (Qiagen), and 20 μl of Proteinase K (Qiagen) to each well and incubated at room temperature for 10 min. Wells were then scrapped and washed twice with the lysate before being collected. Following harvest, the lysate was heated at 56°C for 10 min and then frozen until all time point samples were collected. The remainder of the DNA isolation was performed using the Blood and Tissue Kit (Qiagen).

After DNA isolation was complete, the number of host genome copies and *Chlamydia* genome copies was determined by Droplet Digital PCR (ddPCR) (Hindson *et al.*, 2011). *Chlamydia* genome copies were assessed by the amplification of *secY* and host cell genome copies were assessed by the amplification of *rpp30*. Quantification of copy numbers was determined using Quanta Soft software version 1.7 (Bio-Rad).

Progeny assay

L929 cells were infected with wild-type or RsbU* mutant strains of *C. trachomatis* L2 with BKA (0.25 μM) and HQNO (1 μM) added at the indicated time of infection. At 36 hpi, cells were either fixed and stained using MicroTrack *C. trachomatis* culture confirmation test (Syva Co., Palo Alto, CA) or lysed with water and passaged onto a new monolayer of host cells. An additional 36 h after passaging, the infections were fixed and stained. Fold changes were calculated by counting the IFUs of the infections after the first 36 h and comparing to the IFU counts after the infections were passaged.

Immunofluorescence microscopy

L929 cells were grown to confluency in an 8-well ibiTreat μ-Slide (ibidi, Martinsried, Germany) and were infected with respective wild-type *C. trachomatis* L2, RsbU* mutant, RsbU+ complemented strain, or *ct575*::Tn *bla* strain. Chemical inhibitors (HQNO and BKA) were added to the indicated conditions immediately after infection. At 24 and 72 hpi, infected cells were fixed with 100% methanol for 10 min at room temperature. Cells were washed once with HBSS and again with PBS then stained using 180 μl of the MicroTrack *C. trachomatis* culture confirmation test (Syva Co., Palo Alto, CA) diluted 1:40 in PBS 1 h and 50 min at room temperature. About 20 μl of 1 μM 4′, 6-diamidino-2-phenylindole (DAPI) diluted 1:100 in PBS was then added to wells and allowed to stain for 10 min, room temperature in the dark. The stain was then removed and the cells were washed with PBS. A final overlay of VECTASHIELD Antifade mounting medium (Burlingame, CA) was added and slides were immediately imaged. Cells were visualized on an Olympus IX81/3I spinning disk confocal inverted microscope at 150X magnification and captured on an Andor Zyla 4.2 sCMOS camera (Belfast, Northern Ireland). Microscope and camera were operated using SlideBook 6 software (Intelligent Imaging Innovations, Denver, USA). Exposure time remained consistent for all fields captured, with exposure for DAPI at 2 s, OmpA 3 s and cytoplasm 3 s. Seven *Z*-stack images at 0.3 μm apart were taken per field imaged. Images were processed in SlideBook 6 and a No Neighbors Deconvolution with a subtraction constant of 0.4 was applied to all images. Images represent a maximum projection over the *Z* axis of all seven acquired stacks for each field shown.

Whole-genome sequencing

Chlamydial DNA was extracted from RsbU* EBs. Briefly, 200 μL of renografin-purified EBs were pelleted, resuspended in RQ1 DNase buffer, water and RQ1 DNase, incubated and stopped as per manufacturer's instructions (Promega, Madison, WI). About 2 μL DTT was added to the EBs and DNA was extracted using the Qiagen Blood and Tissue DNA Extraction Kit (Qiagen, catalog number 69506) with the following steps that optimize for DNA sequencing. Libraries were generated using the NEBNext Ultra II DNA Library Prep kit (New England Biolabs, catalog number E7645S). DNA was sequenced by the Illumina Nextseq

MO-SR150bp. Over 91 million reads were generated with a mean quality score of 32.78. Approximately 3% of reads were mapped to the *C. trachomatis* L2/434 (NC_010287) parent genome through reference-guided assembly using the Geneious assembler with up to five iterations. The total average coverage for the RsbU* genome was 400x. Through direct comparison with the reference genome, 33 SNPs were evaluated, including the RsbU* truncation which was confirmed to be a monoclonal polymorphism as 98.6% of reads at that site confirmed the SNP. For the 32 other SNPs discovered in the RsbU* genome, potential effects on secondary structure were analyzed using Geneious secondary structure predictions based on the EMBOSS 6.5.7 tool Garnier or signal cleavage site prediction with sigcleav.

Generation of RsbU complemented mutant (RsbU+) by lateral gene transfer

A confluent layer of Vero monkey kidney cells in a T-75 cell culture flask was infected with 100 μl of RsbU* lysate in 1X SPG buffer. Briefly, the monolayer was washed once with HBSS and 10 ml of HBSS was added to the culture flask along with RsbU* lysate. Cells were spun at 550XG for 30 min at room temperature. Infection material was aspirated from the flask and 15 ml of RPMI containing 1 μg ml⁻¹ of cycloheximide was added to the flask. Infected cells were incubated at 37°C for 85 h postinfection. RsbU* infected cells were then coinfected, as described above, with a *C. trachomatis* mutant containing a transposon insertion in *ct575* (*ct575*::Tn *bla*). Coinfected cells were incubated for another 48 h at 37°C. Cells were then lysed by water lysis and transferred to Vero cell monolayers in a 24-well plate with each well containing variable concentrations of rifampicin and ampicillin to facilitate successful lateral gene transfer of the *bla* resistance marker of the *ct575*::Tn into the RsbU* mutant clone. After 24 hpi, WT-like *Chlamydia* growth was identified by phase-contrast microscopy in a well containing 0.01 μg ml⁻¹ of rifampicin and 5 μg ml⁻¹ of ampicillin. After 32 hpi, cells in the well containing growth were lysed by water and the lysate then underwent two rounds of limiting dilution in a 96-well plate to isolate a clonal population of RsbU complemented mutant recombinants. Mutants with dual antibiotic resistance to rifampicin and ampicillin were evaluated by PCR amplification and sequencing for the genotype of the *rsbU* and *ct163* genes, followed by the other SNPs present in the EMS mutant genome to determine where the area of homologous recombination occurred.

Transcriptional analysis

A confluent monolayer of L929 cells was infected with either WT L2 *C. trachomatis* or the RsbU* mutant strain at an MOI of 1. At 24 hpi, the infections were harvested for RNA using TRIzol (Invitrogen). RNA was purified by phenol/chloroform extraction followed by DNase treatment with TURBO DNase (Invitrogen). A final purification step was performed using the RNeasy Mini Kit (Qiagen) before converting the RNA to cDNA using the High-Capacity cDNA Reverse Transcription Kit (Thermo Fisher). DNA contamination was assessed using a no reverse transcriptase control reaction. After gDNA

depletion has been confirmed for all RNA samples, transcript counts are quantified using ddPCR (Bio-Rad). gDNA taken from the infections was used to normalize the transcript counts.

Conflict of interest

There are no apparent conflicts of interest.

Data availability statement

The data that support the findings of this study are available from the corresponding author upon reasonable request.

References

Adams, P.D., Afonine, P.V., Bunkóczi, G., Chen, V.B., Davis, I.W. and Echols, N., *et al*. (2010) PHENIX: a comprehensive Python-based system for macromolecular structure solution. *Acta Crystallographica. Section D, Biological Crystallography*, **66**(Pt 2), 213–221.

Albe, K.R., Butler, M.H. and Wright, B.E. (1990) Cellular concentrations of enzymes and their substrates. *Journal of Theoretical Biology*, **143**(2), 163–195.

Belland, R.J., Zhong, G., Crane, D.D., Hogan, D., Sturdevant, D., Sharma, J., *et al*. (2003) Genomic transcriptional profiling of the developmental cycle of *Chlamydia trachomatis*. *Proceedings of the National Academy of Sciences of the United States of America*, **100**(14), 8478–8483.

Benson, A.K. and Haldenwang, W.G. (1993) Regulation of sigma B levels and activity in *Bacillus subtilis*. *Journal of Bacteriology*, **175**(8), 2347–2356.

Brothwell, J.A., Muramatsu, M.K., Toh, E., Rockey, D.D., Putman, T.E., Barta, M.L., *et al*. (2016) Interrogating genes that mediate *Chlamydia trachomatis* survival in cell culture using conditional mutants and recombination. *Journal of Bacteriology*, **198**(15), 2131–2139.

Bryant, S.H. and Altschul, S.F. (1995) Statistics of sequence-structure threading. *Current Opinion in Structural Biology*, **5**(2), 236–244.

Caspi, R., Billington, R., Ferrer, L., Foerster, H., Fulcher, C.A., Keseler, I.M., *et al*. (2016) The MetaCyc database of metabolic pathways and enzymes and the BioCyc collection of pathway/genome databases. *Nucleic Acids Research*, **44**(D1), D471–D480.

Chang, C., Tesar, C., Gu, M., Babnigg, G., Joachimiak, A., Pokkuluri, P.R., *et al*. (2010) Extracytoplasmic PAS-like domains are common in signal transduction proteins. *Journal of Bacteriology*, **192**(4), 1156–1159.

Chen, V.B., Arendall, W.B., Headd, J.J., Keedy, D.A., Immormino, R.M., Kapral, G.J., *et al*. (2010) MolProbity: all-atom structure validation for macromolecular crystallography. *Acta Crystallographica. Section D, Biological Crystallography*, **66**(Pt 1), 12–21.

Cheung, J. and Hendrickson, W.A. (2008) Crystal structures of C4-dicarboxylate ligand complexes with sensor domains of histidine kinases DcuS and DctB. *Journal of Biological Chemistry*, **283**(44), 30256–30265.

Claywell, J.E., Matschke, L.M., Plunkett, K.N. and Fisher, D.J. (2018) Inhibition of the protein phosphatase CppA alters development of *Chlamydia trachomatis*. *Journal of Bacteriology*, **200**(19), e00419-18.

Coordinators, N.R. (2017) Database resources of the national center for biotechnology information. *Nucleic Acids Research*, **45**(Database), D12.

Delumeau, O., Dutta, S., Brigulla, M., Kuhnke, G., Hardwick, S.W., Völker, U., *et al*. (2004) Functional and structural characterization of RsbU, a stress signaling protein phosphatase 2C. *Journal of Biological Chemistry*, **279**(39), 40927–40937.

Diederichs, K. and Karplus, P.A. (1997) Improved R-factors for diffraction data analysis in macromolecular crystallography. *Nat Struct Biol*, **4**(4), 269–275.

Douglas, A.L. and Hatch, T.P. (2000) Expression of the transcripts of the sigma factors and putative sigma factor regulators of *Chlamydia trachomatis* L2. *Gene*, **247**(1–2), 209–214.

Elliott, K.T., Zhulin, I.B., Stuckey, J.A. and DiRita, V.J. (2009) Conserved residues in the HAMP domain define a new family of proposed bipartite energy taxis receptors. *Journal of Bacteriology*, **191**(1), 375–387.

Elwell, C., Mirrashidi, K. and Engel, J. (2016) Chlamydia cell biology and pathogenesis. *Nature Reviews Microbiology*, **14**(6), 385–400.

Emsley, P., Lohkamp, B., Scott, W.G. and Cowtan, K. (2010) Features and development of Coot. *Acta Crystallographica. Section D, Biological Crystallography*, **66**(Pt 4), 486–501.

Evans, P. (2006) Scaling and assessment of data quality. *Acta Crystallogr D Biol Crystallogr*, **62**(Pt 1), 72–82.

Evans, P.R. (2011) An introduction to data reduction: space-group determination, scaling and intensity statistics. *Acta Crystallographica. Section D, Biological Crystallography*, **67**(Pt 4), 282–292.

Fisher, D.J., Adams, N.E. and Maurelli, A.T. (2015) Phosphoproteomic analysis of the *Chlamydia caviae*

elementary body and reticulate body forms. *Microbiology*, **161**(8), 1648–1658.

Friesner, R.A., Banks, J.L., Murphy, R.B., Halgren, T.A., Klicic, J.J. and Mainz, D.T., *et al.* (2004) Glide: a new approach for rapid, accurate docking and scoring. 1. Method and assessment of docking accuracy. *Journal of Medicinal Chemistry*, **47**(7), 1739–1749.

Friesner, R.A., Murphy, R.B., Repasky, M.P., Frye, L.L., Greenwood, J.R., Halgren, T.A., *et al.* (2006) Extra precision glide: docking and scoring incorporating a model of hydrophobic enclosure for protein-ligand complexes. *Journal of Medicinal Chemistry*, **49**(21), 6177–6196.

Hackstadt, T., Todd, W.J. and Caldwell, H.D. (1985) Disulfide-mediated interactions of the chlamydial major outer membrane protein: role in the differentiation of chlamydiae? *Journal of Bacteriology*, **161**(1), 25–31.

Halgren, T.A., Murphy, R.B., Friesner, R.A., Beard, H.S., Frye, L.L., Pollard, W.T., *et al.* (2004) Glide: a new approach for rapid, accurate docking and scoring. 2. Enrichment factors in database screening. *Journal of Medicinal Chemistry*, **47**(7), 1750–1759.

Hatch, T.P., Allan, I. and Pearce, J.H. (1984) Structural and polypeptide differences between envelopes of infective and reproductive life cycle forms of *Chlamydia* spp. *Journal of Bacteriology*, **157**(1), 13–20.

Hawkins, P.C.D., Skillman, A.G., Warren, G.L., Ellingson, B.A. and Stahl, M.T. (2010) Conformer generation with OMEGA: algorithm and validation using high quality structures from the Protein Databank and Cambridge Structural Database. *Journal of Chemical Information and Modeling*, **50**(4), 572–584.

Hecker, M., Pane-Farre, J. and Volker, U. (2007) SigB-dependent general stress response in *Bacillus subtilis* and related gram-positive bacteria. *Annual Review of Microbiology*, **61**, 215–236.

Hindson, B.J., Ness, K.D., Masquelier, D.A., Belgrader, P., Heredia, N.J., Makarewicz, A.J., *et al.* (2011) High-throughput droplet digital PCR system for absolute quantitation of DNA copy number. *Analytical Chemistry*, **83**(22), 8604–8610.

Hua, L., Hefty, P.S., Lee, Y.J., Lee, Y.M., Stephens, R.S. and Price, C.W. (2006) Core of the partner switching signalling mechanism is conserved in the obligate intracellular pathogen *Chlamydia trachomatis*. *Molecular Microbiology*, **59**(2), 623–636.

Hughes, K.T. and Mathee, K. (1998) The anti-sigma factors. *Annual Review of Microbiology*, **52**, 231–286.

Hulko, M., Berndt, F., Gruber, M., Linder, J.U., Truffault, V., Schultz, A., *et al.* (2006) The HAMP domain structure implies helix rotation in transmembrane signaling. *Cell*, **126**(5), 929–940.

Iliffe-Lee, E.R. and McClarty, G. (1999) Glucose metabolism in *Chlamydia trachomatis*: the 'energy parasite' hypothesis revisited. *Molecular Microbiology*, **33**(1), 177–187.

Iliffe-Lee, E.R. and McClarty, G. (2000) Regulation of carbon metabolism in *Chlamydia trachomatis*. *Molecular Microbiology*, **38**(1), 20–30.

Jacobson, M.P., Friesner, R.A., Xiang, Z. and Honig, B. (2002) On the role of the crystal environment in determining protein side-chain conformations. *Journal of Molecular Biology*, **320**(3), 597–608.

Jacobson, M.P., Pincus, D.L., Rapp, C.S., Day, T.J.F., Honig, B., Shaw, D.E., *et al.* (2004) A hierarchical approach to all-atom protein loop prediction. *Proteins*, **55**(2), 351–367.

Janausch, I., Zientz, E., Tran, Q., Kröger, A. and Unden, G. (2002) C4-dicarboxylate carriers and sensors in bacteria. *Biochimica et Biophysica Acta*, **1553**(1–2), 39–56.

Jason-Moller, L., Murphy, M. and Bruno, J. (2006) Overview of Biacore systems and their applications. *Current Protocols in Protein Science*, **45**(1), Unit 19–13.

Kabsch, W. and Sander, C. (1983) Dictionary of protein secondary structure: pattern recognition of hydrogen-bonded and geometrical features. *Biopolymers*, **22**(12), 2577–2637.

Kang, C.M., Brody, M.S., Akbar, S., Yang, X. and Price, C.W. (1996) Homologous pairs of regulatory proteins control activity of *Bacillus subtilis* transcription factor sigma(b) in response to environmental stress. *Journal of Bacteriology*, **178**(13), 3846–3853.

Kang, C.M., Vijay, K. and Price, C.W. (1998) Serine kinase activity of a *Bacillus subtilis* switch protein is required to transduce environmental stress signals but not to activate its target PP2C phosphatase. *Molecular Microbiology*, **30**(1), 189–196.

Kokes, M., Dunn, J.D., Granek, J.A., Nguyen, B.D., Barker, J.R, Valdivia, R.H., *et al.* (2015) Integrating chemical mutagenesis and whole-genome sequencing as a platform for forward and reverse genetic analysis of Chlamydia. *Cell Host & Microbe*, **17**(5), 716–725.

Kozak, N.A., Mattoo, S., Foreman-Wykert, A.K., Whitelegge, J.P. and Miller, J.F. (2005) Interactions between partner switcher orthologs BtrW and BtrV regulate type III secretion in Bordetella. *Journal of Bacteriology*, **187**(16), 5665–5676.

Krissinel, E. (2012) Enhanced fold recognition using efficient short fragment clustering. *Journal of Molecular Biochemistry*, **1**(2), 76–85.

Langer, G., Cohen, S.X., Lamzin, V.S. and Perrakis, A. (2008) Automated macromolecular model building for X-ray crystallography using ARP/wARP version 7. *Nature Protocols*, **3**(7), 1171–1179.

Liang, P., Rosas-Lemus, M., Patel, D., Fang, X., Tuz, K. and Juárez, O. (2018) Dynamic energy dependency of *Chlamydia trachomatis* on host cell metabolism during intracellular growth: role of sodium-based energetics in chlamydial ATP generation. *Journal of Biological Chemistry*, **293**(2), 510–522.

Liechti, G.W., Kuru, E., Hall, E., Kalinda, A., Brun, Y.V., VanNieuwenhze, M., *et al.* (2014) A new metabolic cell-wall labelling method reveals peptidoglycan in *Chlamydia trachomatis*. *Nature*, **506**(7489), 507–510.

Liu, J., Yang, J., Wen, J., Yang, Y., Wei, X., Zhang, X., *et al.* (2014) Mutational analysis of dimeric linkers in peri- and cytoplasmic domains of histidine kinase DctB reveals their functional roles in signal transduction. *Open Biology*, **4**(6), 140023.

Liu, Y.C., Machuca, M.A., Beckham, S.A., Gunzburg, M.J. and Roujeinikova, A. (2015) Structural basis for amino-acid recognition and transmembrane signalling by tandem Per-Arnt-Sim (tandem PAS) chemoreceptor sensory domains. *Acta Crystallographica. Section D, Biological Crystallography*, **71**(Pt 10), 2127–2136.

Matthews, B.W. (1968) Solvent content of protein crystals. *Journal of Molecular Biology*, **33**(2), 491–497.

Mattoo, S., Yuk, M.H., Huang, L.L. and Miller, J.F. (2004) Regulation of type III secretion in Bordetella. *Molecular Microbiology*, **52**(4), 1201–1214.

McCoy, A.J., Grosse-Kunstleve, R.W., Adams, P.D., Winn, M.D., Storoni, L.C. and Read, R.J. (2007) Phaser crystallographic software. *Journal of Applied Crystallography*, **40**(Pt 4), 658–674.

McGann, M. (2011) FRED pose prediction and virtual screening accuracy. *Journal of Chemical Information and Modeling*, **51**(3), 578–596.

Mehlitz, A., Eylert, E., Huber, C., Lindner, B., Vollmuth, N., Karunakaran, K., *et al.* (2017) Metabolic adaptation of *Chlamydia trachomatis* to mammalian host cells. *Molecular Microbiology*, **103**(6), 1004–1019.

Morris, A.R. and Visick, K.L. (2013) The response regulator SypE controls biofilm formation and colonization through phosphorylation of the syp-encoded regulator SypA in *Vibrio fischeri*. *Molecular Microbiology*, **87**(3), 509–525.

Nan, B., Liu, X., Zhou, Y., Liu, J., Zhang, L., Wen, J., *et al.* (2010) From signal perception to signal transduction: ligand-induced dimeric switch of DctB sensory domain in solution. *Molecular Microbiology*, **75**(6), 1484–1494.

Nguyen, B.D. and Valdivia, R.H. (2012) Virulence determinants in the obligate intracellular pathogen *Chlamydia trachomatis* revealed by forward genetic approaches. *Proceedings of the National Academy of Sciences of the United States of America*, **109**(4), 1263–1268.

Nguyen, M.N., Tan, K.P. and Madhusudhan, M.S. (2011) CLICK–topology-independent comparison of biomolecular 3D structures. *Nucleic Acids Research*, **39**(Supplement 2), W24–W28.

Nicholson, T.L., Olinger, L., Chong, K., Schoolnik, G. and Stephens, R.S. (2003) Global stage-specific gene regulation during the developmental cycle of *Chlamydia trachomatis*. *Journal of Bacteriology*, **185**(10), 3179–3189.

Niesen, F.H., Berglund, H. and Vedadi, M. (2007) The use of differential scanning fluorimetry to detect ligand interactions that promote protein stability. *Nature Protocols*, **2**(9), 2212–2221.

Nishiyama, S.I., Takahashi, Y., Yamamoto, K., Suzuki, D., Itoh, Y. and Sumita, K., *et al.* (2016) Identification of a *Vibrio cholerae* chemoreceptor that senses taurine and amino acids as attractants. *Scientific Reports*, **6**, 20866.

O'Hearn, S.D., Kusalik, A.J. and Angel, J.F. (2003) MolCom: a method to compare protein molecules based on 3-D structural and chemical similarity. *Protein Engineering*, **16**(3), 169–178.

Packiam, M., Weinrick, B., Jacobs, W.R. and Maurelli, A.T. (2015) Structural characterization of muropeptides from *Chlamydia trachomatis* peptidoglycan by mass spectrometry resolves 'chlamydial anomaly'. *Proceedings of the National Academy of Sciences of the United States of America*, **112**(37), 11660–11665.

Paget, M.S. (2015) Bacterial sigma factors and anti-sigma factors: structure, function and distribution. *Biomolecules*, **5**(3), 1245–1265.

Painter, J. and Merritt, E.A. (2006) Optimal description of a protein structure in terms of multiple groups undergoing TLS motion. *Acta Crystallographica. Section D, Biological Crystallography*, **62**(Pt 4), 439–450.

Pilhofer, M., Aistleitner, K., Biboy, J., Gray, J., Kuru, E. and Hall, E., *et al.* (2013) Discovery of chlamydial peptidoglycan reveals bacteria with murein sacculi but without FtsZ. *Nature Communications*, **4**, 2856.

Rahman, H., King, R.M., Shewell, L.K., Semchenko, E.A., Hartley-Tassell, L.E., Wilson, J.C., *et al.* (2014) Characterisation of a multi-ligand binding chemoreceptor CcmL (Tlp3) of *Campylobacter jejuni*. *PLoS Pathogens*, **10**(1), e1003822.

Rico-Jiménez, M., Muñoz-Martínez, F., García-Fontana, C., Fernandez, M., Morel, B., Ortega, Á., *et al.* (2013) Paralogous chemoreceptors mediate chemotaxis towards protein amino acids and the non-protein amino acid gamma-aminobutyrate (GABA). *Molecular Microbiology*, **88**(6), 1230–1243.

Schultz, J., Milpetz, F., Bork, P. and Ponting, C.P. (1998) SMART, a simple modular architecture research tool: identification of signaling domains. *Proceedings of the National Academy of Sciences of the United States of America*, **95**(11), 5857–5864.

Shi, Y. (2009) Serine/threonine phosphatases: mechanism through structure. *Cell*, **139**(3), 468–484.

Stephens, R.S., Kalman, S., Lammel, C., Fan, J., Marathe, R. and Aravind, L., *et al.* (1998) Genome sequence of an obligate intracellular pathogen of humans: *Chlamydia trachomatis*. *Science*, **282**(5389), 754–759.

Thompson, C.C., Griffiths, C., Nicod, S.S., Lowden, N.M., Wigneshweraraj, S., Fisher, D.J., *et al.* (2015) The Rsb phosphoregulatory network controls availability of the primary sigma factor in *Chlamydia trachomatis* and influences the kinetics of growth and development. *PLoS Pathogens*, **11**(8), e1005125.

Tjaden, J., Winkler, H.H., Schwöppe, C., Van Der Laan, M., Möhlmann, T. and Neuhaus, H.E. (1999) Two nucleotide transport proteins in *Chlamydia trachomatis*, one for net nucleoside triphosphate uptake and the other for transport of energy. *Journal of Bacteriology*, **181**(4), 1196–1202.

Tuz, K., Mezic, K.G., Xu, T., Barquera, B. and Juarez, O. (2015) The kinetic reaction mechanism of the *Vibrio cholerae* sodium-dependent NADH dehydrogenase. *Journal of Biological Chemistry*, **290**(33), 20009–20021.

Voelker, U., Voelker, A., Maul, B., Hecker, M., Dufour, A. and Haldenwang, W.G. (1995b) Separate mechanisms activate sigma B of *Bacillus subtilis* in response to environmental and metabolic stresses. *Journal of Bacteriology*, **177**(13), 3771–3780.

Voelker, U., Dufour, A. and Haldenwang, W.G. (1995a) The *Bacillus subtilis* rsbU gene product is necessary for RsbX-dependent regulation of sigma B. *Journal of Bacteriology*, **177**(1), 114–122.

Vonrhein, C., Flensburg, C., Keller, P., Sharff, A., Smart, O., Paciorek, W., *et al.* (2011) Data processing and analysis with the autoPROC toolbox. *Acta Crystallographica. Section D, Biological Crystallography*, **67**(Pt 4), 293–302.

Weber, A., Menzlaff, E., Arbinger, B., Gutensohn, M., Eckerskorn, C. and Fluegge, U.-I. (1995) The 2-oxoglutarate/malate translocator of chloroplast envelope membranes: molecular cloning of a transporter containing a 12-helix motif and expression of the functional protein in yeast cells. *Biochemistry*, **34**(8), 2621–2627.

Weiss, M. (2001) Global indicators of X-ray data quality. *J Appl Crystallogr*, **34**, 130–135.

Winkler, H.H. and Neuhaus, H.E. (1999) Non-mitochondrial ATP transport. *Trends in Biochemical Sciences*, **24**(2), 64–68.

Winn, M.D., Ballard, C.C., Cowtan, K.D., Dodson, E.J., Emsley, P., Evans, P.R., *et al.* (2011) Overview of the CCP4 suite and current developments. *Acta Crystallographica. Section D, Biological Crystallography*, **67**(Pt 4), 235–242.

Winn, M.D., Isupov, M.N. and Murshudov, G.N. (2001) Use of TLS parameters to model anisotropic displacements in macromolecular refinement. *Acta Crystallographica. Section D, Biological Crystallography*, **57**(Pt 1), 122–133.

Wise, A.A. and Price, C.W. (1995) Four additional genes in the sigB operon of *Bacillus subtilis* that control activity of the general stress factor sigma B in response to environmental signals. *Journal of Bacteriology*, **177**(1), 123–133.

Wishart, D.S., Knox, C., Guo, A.C., Eisner, R., Young, N., Gautam, B., *et al.* (2009) HMDB: a knowledgebase for the human metabolome. *Nucleic Acids Research*, **37**(Database), D603–D610.

Wishart, D.S., Tzur, D., Knox, C., Eisner, R., Guo, A.C., Young, N., *et al.* (2007) HMDB: the human metabolome database. *Nucleic Acids Research*, **35**(Database), D521–D526.

Wishart, D.S., Feunang, Y.D., Marcu, A., Guo, A.C., Liang, K., Vázquez-Fresno, R., *et al.* (2018) HMDB 4.0: the human metabolome database for 2018. *Nucleic Acids Research*, **46**(D1), D608–D617.

Wu, R., Gu, M., Wilton, R., Babnigg, G., Kim, Y. and Pokkuluri, P.R., *et al.* (2013) Insight into the sporulation phosphorelay: crystal structure of the sensor domain of *Bacillus subtilis* histidine kinase, KinD. *Protein Science*, **22**(5), 564–576.

Xu, J. and Zhang, Y. (2010) How significant is a protein structure similarity with TM-score = 0.5? *Bioinformatics*, **26**(7), 889–895.

Yang, X., Kang, C.M., Brody, M.S. and Price, C.W. (1996) Opposing pairs of serine protein kinases and phosphatases transmit signals of environmental stress to activate a bacterial transcription factor. *Genes & Development*, **10**(18), 2265–2275.

Yang, J., Yan, R., Roy, A., Xu, D., Poisson, J. and Zhang, Y. (2015) The I-TASSER Suite: protein structure and function prediction. *Nature Methods*, **12**(1), 7–8.

Yu, H.H. and Tan, M. (2003) Sigma28 RNA polymerase regulates hctB, a late developmental gene in Chlamydia. *Molecular Microbiology*, **50**(2), 577–584.

Zhang, W., Yang, J., He, B., Walker, S.E., Zhang, H., Govindarajoo, B., *et al.* (2016) Integration of QUARK and I-TASSER for ab initio protein structure prediction in CASP11. *Proteins*, **84** (Supplement 1), 76–86.

Zhang, Z. and Hendrickson, W.A. (2010) Structural characterization of the predominant family of histidine kinase sensor domains. *Journal of Molecular Biology*, **400**(3), 335–353.

Zhang, Y. and Skolnick, J. (2004) Scoring function for automated assessment of protein structure template quality. *Proteins*, **57**(4), 702–710.

Zhang, Y. and Skolnick, J. (2005) TM-align: a protein structure alignment algorithm based on the TM-score. *Nucleic Acids Research*, **33**(7), 2302–2309.

Zhou, Y.F., Nan, B., Nan, J., Ma, Q., Panjikar, S., Liang, Y.H., *et al.* (2008) C4-dicarboxylates sensing mechanism revealed by the crystal structures of DctB sensor domain. *Journal of Molecular Biology*, **383**(1), 49–61.

Zhulin, I.B., Nikolskaya, A.N. and Galperin, M.Y. (2003) Common extracellular sensory domains in transmembrane receptors for diverse signal transduction pathways in bacteria and archaea. *Journal of Bacteriology*, **185**(1), 285–294.

Supporting Information

Additional supporting information may be found online in the Supporting Information section at the end of the article